Available online at www.sciencedirect.com
ScienceDirect
Comput. Methods Appl. Mech. Engrg. 196 (2006) 665–681
Computer methods in applied mechanics and engineering
www.elsevier.com/locate/cma

Time-dependent Maxwell's equations with charges in singular geometries

F. Assous [a,b,*], P. Ciarlet Jr. [c], E. Garcia [c], J. Segré [d]

[a] Bar-Ilan University, Department of Mathematics and Statistics, 52900 Ramat-Gan, Israel
[b] College of Judea & Samaria, Department of Mathematics and Computer Sciences, 44837 Ariel, Israel
[c] ENSTA & CNRS UMR 2706, 32 boulevard Victor, 75739 Paris Cedex 15, France
[d] CEN Saclay, DANS/DM2S/SFME, 91691 Gif-sur-Yvette Cedex, France

Received 30 December 2004; received in revised form 17 January 2006; accepted 5 July 2006

Abstract

This paper is devoted to the solution of the instationary Maxwell equations with charges. The geometry of the domain can be singular, in the sense that its boundary can include reentrant corners or edges. The difficulties arise from the fact that those geometrical singularities generate, in their neighborhood, strong electromagnetic fields. The time-dependency of the divergence of the electric field, is addressed. To tackle this problem, some new theoretical and practical results are presented, on curl-free singular fields, and on singular fields with L^2 (non-vanishing) divergence. The method, which allows to compute the instationary electromagnetic field, is based on a splitting of the spaces of solutions into a two-term direct sum. First, the subspace of regular fields: it coincides with the whole space of solutions, provided that the domain is either convex, or with a smooth boundary. Second, a singular subspace, defined and characterized via the singularities of the Laplace operator. Several numerical examples are presented, to illustrate the mathematical framework. This paper is the generalization of the *singular complement method*.

Keywords: Maxwell equations; Singular geometries; Continuous finite element methods

0. Introduction

Many practical problems require the computation of electromagnetic fields. They are usually based on Maxwell equations. In a number of applications, such as plasma physics or hyperfrequency devices, the right-hand sides of those equations model charge and current densities, which are also unknowns of the problem. These Maxwell right-hand sides are computed by solving the Vlasov equation, or one of its simplified models. Thus, the complete set of unknowns – electromagnetic field, current and charge densities – is the solution of the coupled Vlasov–Maxwell equations.

Within this framework, we developed a numerical method for solving the instationary Maxwell equations (see [10]), with continuous approximations of the electromagnetic field. As a matter of fact, providing a continuous approximation is recommended by Birdsall and Langdon [14], in order to reduce spurious oscillations in the numerical solution of the coupled Vlasov–Maxwell equations. In addition, the time-stepping numerical scheme, which is explicit by construction, can be solved very efficiently. One does not have to compute the solution of a linear system at each time step: diagonal matrix-vector multiplications are sufficient. Finally, in order to handle precisely the conditions on the divergence of the fields, these are considered as constraints. They are dualized, using a Lagrange multiplier, which yields a saddle-point variational formulation.

In practical examples, the boundary of the computational domain includes reentrant corners and/or edges.

* Corresponding author.
E-mail address: franckassous@netscape.net (F. Assous).

0045-7825/$ - see front matter © 2006 Elsevier B.V. All rights reserved.
doi:10.1016/j.cma.2006.07.007

They are called *geometrical singularities* and, as far as electromagnetic fields are concerned, they generate strong fields. Those singularities can be either active or passive. Active, in the sense that they are included on purpose, to generate strong fields. Passive, when they are the result of exterior constraints, which can occur for instance in the design of the device. In any case, the presence of these geometrical singularities requires a careful computation of the electromagnetic field in their neighborhood. Indeed, for an instationary problem, the propagative nature of the solution magnifies the errors, including those generated near the singularities.

Several approaches have been proposed in the literature, for solving Maxwell equations in a domain with geometrical singularities. To our knowledge, the first theoretical works on this topic are those of Birman and Solomyak [15–17], who studied the domain of the Maxwell operator, so that it is self-adjoint in $\mathbf{L}^2(\Omega)$ (with $\Omega \subset \mathbb{R}^3$). Then, and most important for on own purposes, they proved a splitting of the space of electromagnetic fields into a two-term *simple* sum. First, the subspace of regular fields. Second, the subspace made of gradients of solutions to the Laplace problem.

During the 1990s, Costabel and Dauge [34,29–32] provided new insight on the characterizations of the singularities of the electromagnetic fields, called afterwards electromagnetic singularities. In addition, they proved density results, and carried out a careful description of the Maxwell operator in 2D and 3D. Recently [33], they proposed that the electric field be fully taken into account – without any splitting – thanks to a technique which consists in introducing suitable *weights* in the definition of functional spaces: it allows to capture numerically strong electric fields.

We refer to the work of Bonnet-Ben Dhia et al. [18] and Lohrengel [47], for solving the time-harmonic, divergence-free Maxwell equations. They used a *regularized* formulation, and proposed a numerical implementation relying on a truncation function. But, in practice, this truncation function generated a very slow numerical convergence, so they introduced an alternative approach (cf. [43]), which proved to be more efficient.

Finally, we mention comparisons of different existing approaches for solving the 2D Maxwell equations in [42,45].

We developed a method, the so-called *singular complement method* (referred to as the *SCM* hereafter), which consists in splitting the space of electric fields, $\mathbf{X}$, into a two-term, *direct*, possibly *orthogonal* sum. The first subspace, $\mathbf{X}_\mathbf{R}$, is made of regular fields. The second one, $\mathbf{X}_\mathbf{S}$, is called the subspace of *singular electric fields*. The subspace $\mathbf{X}_\mathbf{R}$ coincides with the whole space of solutions, provided that the domain is either convex, or with a smooth boundary. So, one can compute the regular part of the solution with the help of an ad hoc – classical – method [10]. The singular part is computed with the help of specifically designed methods: they originate from relations between the electromagnetic singularities and the singularities of the Laplace operator. Note that the same ideas carry over to the magnetic field.

The present paper can be viewed as a continuation of this idea. We refer the interested reader to [9,8,2,7], dealing with the 2D or 3D divergence-free Maxwell equations. We also refer the reader to [23,46] for extensions of the *SCM* to some 3D cases: in prismatic domains, or in domains invariant by rotation.

When the divergence of the electric field no longer vanishes, $\mathrm{div}\mathscr{E} = f(t)$, with $f \neq 0$, one can substract a gradient, to reach the divergence-free field

$$\widetilde{\mathscr{E}} = \mathscr{E} - \mathrm{grad}\phi.$$

Still, to determine ϕ, one has to solve the time-dependent (via the data) problem

$$-\Delta\phi = f(t),$$

which slows down drastically the numerical implementation. To alleviate this drawback, we study in detail different splittings of the electromagnetic space, which could be used for the *SCM*. Hence, we propose new splittings, direct and possibly orthogonal, with curl-free singular fields, or with singular fields with L^2 divergence. The relations between those different splittings allow to understand better the structure of electromagnetic singularities. The main new results can be summarized as follows:

- The introduction of new splittings, which are proven to be *equivalent*, as far as the principal part of the singularities are concerned. It should be noted that those splittings, although they yield comparable numerical results, are not equally easy to implement. As a matter of fact, for each splitting, the singular subspace is characterized differently, which leads to (noticeable) differences in computing the regular and singular parts of the field. Thus, the choice of the splitting will depend mainly on the numerical implementation.
- The numerical algorithms for the computation of the electromagnetic field in 3D domains. First, when the geometrical singularities generate a finite dimensional singular subspace. The chosen geometrical singularity is called a *sharp conical vertex* (see [6] and references therein). Second, we also describe how one can construct algorithms to compute the field in 3D prismatic, or 3D invariant by rotation, domains. In these domains, the singular subspaces are usually *infinite dimensional*.
- As an important application – actually, the origin of this study – we present the computation of strong electromagnetic fields, via the numerical solution to the coupled, non-linear, Vlasov–Maxwell system of equations.

The paper is organized as follows. In Section 1, we recall Maxwell equations, together with the functional framework, which is then used to describe the *singular complement method*. We focus on regular/singular splittings, and on mappings, which allow to characterize the singular electromagnetic fields with a non-vanishing divergence. Section 2 is devoted to the numerical algorithms. In particular, the computation of singular basis functions is described,

together with the discretization of the variational formulations. Error estimates are provided in 2D. And finally, a discussion of the 3D implementations is addressed. Numerical experiments are presented in Section 3. First, the (non-) influence of the different splittings is established numerically. Then, a numerical implementation of the coupled Vlasov–Maxwell system is considered.

Instead of writing "in a convex domain, or in a domain with a smooth boundary (of regularity at least $C^{1,1}$)", we simply write "in a convex domain". Correspondingly, "in a non-convex domain" means "in a non-convex domain, with a non-smooth boundary", that is in a domain with geometrical singularities.

1. Theory

1.1. Instationary Maxwell equations

Let Ω be a bounded, open, polyhedral subset of $\mathbb{R}^3$. Let Γ be its boundary, which we assume to be Lipschitz continuous and connected. Then, denote by $\mathbf{n}$ the unit outward normal to Γ. If we let c, ε_0 and μ_0 be respectively the light velocity, the dielectric permittivity and the magnetic permeability ($\varepsilon_0\mu_0c^2 = 1$), Maxwell equations in vacuum read,

$$\begin{aligned}
&\frac{\partial \mathscr{E}}{\partial t} - c^2\mathbf{curl}\mathscr{B} = -\frac{1}{\varepsilon_0}\mathscr{J},\\
&\frac{\partial \mathscr{B}}{\partial t} + \mathbf{curl}\mathscr{E} = 0,\\
&\mathrm{div}\mathscr{E} = \frac{\rho}{\varepsilon_0},\\
&\mathrm{div}\mathscr{B} = 0,
\end{aligned}$$

where $\mathscr{E}$ and $\mathscr{H}$ are the electric and magnetic fields, ρ and $\mathscr{J}$ the charge and current densities. These quantities depend on the space variable $\mathbf{x}$ and on the time variable t. The charge conservation reads

$$\frac{\partial \rho}{\partial t} + \mathrm{div}\mathscr{J} = 0.$$

These equations are supplemented with appropriate boundary conditions. For simplicity reasons, let us assume first that the boundary Γ corresponds to the interface with a perfectly conducting body. This results in the perfect conducting boundary conditions

$$\mathscr{E} \times \mathbf{n} = 0 \quad \text{and} \quad \mathscr{B} \cdot \mathbf{n} = 0 \quad \text{on } \Gamma.$$

In Section 1.4, the boundary Γ is split into two parts. A perfect conducting boundary, and an artificial boundary, on which a Silver–Müller absorbing boundary condition is imposed. This allows to model either incoming plane waves, or the absorption of outgoing waves. Finally, one adds initial conditions, set at time $t = 0$,

$$\mathscr{E}(0) = \mathscr{E}_0, \quad \mathscr{B}(0) = \mathscr{B}_0.$$

The electromagnetic field $(\mathscr{E}_0, \mathscr{B}_0)$ depends only on the space variables, and it satisfies

$$\begin{aligned}
&\mathrm{div}\mathscr{E}_0 = \frac{\rho(0)}{\varepsilon_0}, \quad \mathrm{div}\mathscr{B}_0 = 0,\\
&\mathscr{E}_0 \times \mathbf{n} = 0 \quad \text{in } \Gamma, \quad \mathscr{B}_0 \cdot \mathbf{n} = 0 \quad \text{in } \Gamma.
\end{aligned}$$

It is also possible to write down Maxwell equations in 2D. Assume that the problem is formally set in an infinite cylinder Ω, and that the domain, the field and the data – $\mathscr{E}, \mathscr{B}, \mathscr{J}, \rho, \mathscr{E}_0, \mathscr{B}_0$ – are all independent of one of the three space variables (x, y, z), let us say z. Then, one can consider an equivalent problem, in a 2D section of Ω, perpendicular to the axis Oz [3]. Let $\Omega_\perp$ denote the 2D section, and let $\Gamma_\perp$ be its boundary. Denote further by $\boldsymbol{\nu}$ the unit outward normal to $\Gamma_\perp$, and by $\boldsymbol{\tau}$ the unit tangent vector such that $(\boldsymbol{\tau},\boldsymbol{\nu})$ is direct.

In $\mathbb{R}^2$, there exist two curl operators: the first one is scalar and acts on vector fields, whereas the second one is vector and acts on scalar fields. We denote them respectively by *curl* and $\mathbf{curl}_\perp$. The divergence and gradient are defined classically.

For a 3D vector field $\mathscr{U}$, let $\mathscr{U}_\perp = (\mathscr{U}_x, \mathscr{U}_y)$ be the transverse components. The above assumptions yield

$$\mathbf{curl}\mathscr{U} = \begin{pmatrix} \mathbf{curl}_\perp \mathscr{U}_z \\ curl\,\mathscr{U}_\perp \end{pmatrix} \quad \text{and} \quad \mathbf{curl}\,\mathbf{curl}\mathscr{U} = \begin{pmatrix} \mathbf{curl}_\perp curl\,\mathscr{U}_\perp \\ -\Delta\mathscr{U}_z \end{pmatrix}. \tag{1}$$

Remark 1.1. We shall not consider invariance by rotation, which corresponds to the axisymmetric case. Results are somewhat similar, but the techniques of proof are very different. We refer the reader to [5] and references therein.

In what follows, when we write results in 3D only, it is understood that they carry out to 2D. When it is not the case, we state both the 3D and 2D results.

1.2. The singular complement method

Let us define some functional spaces, which are used throughout the paper. From the functional analysis point of view, the electric and magnetic formulations are very similar and present the same mathematical structure. As we are interested in non-divergence-free solutions, especially in Vlasov–Maxwell equations, we only present the electric formulation. Details on the magnetic counterpart can be found in [36].

First, we introduce the space of electric fields $\mathscr{E}$, called $\mathbf{X}$, and its divergence- or curl-free subspaces $\mathbf{V}$ and $\mathbf{L}$,

$$\begin{aligned}
&\mathbf{X} = \{\mathbf{x} \in \mathbf{H}(\mathbf{curl}, \Omega) \cap \mathbf{H}(\mathrm{div}, \Omega) \ : \ \mathbf{x} \times \mathbf{n}_{|\Gamma} = 0\},\\
&\mathbf{V} = \{\mathbf{v} \in \mathbf{X}, \mathrm{div}\,\mathbf{v} = 0\}, \quad \mathbf{L} = \{\mathbf{l} \in \mathbf{X}, \mathbf{curl}\,\mathbf{l} = 0\}.
\end{aligned}$$

This definition of $\mathbf{X}$ assumes that the charge density ρ is square integrable. Spaces of potentials are also useful, such as the one which corresponds to the solutions to the

Laplace problem with L^2 right-hand side, and homogeneous Dirichlet boundary condition,

$$\Psi = \{\psi \in H_0^1(\Omega),\ \Delta\psi \in L^2(\Omega)\}.$$

Above, $H_0^1(\Omega)$ is the subspace of $H^1(\Omega)$, the elements of which have a vanishing trace.

All spaces are a priori equipped with the natural, induced, norm, i.e. for $\mathbf{X}$ the norm of $\mathbf{H}(\mathbf{curl},\Omega) \cap \mathbf{H}(\mathrm{div},\Omega)$, for $\mathbf{V}$ the norm of $\mathbf{H}(\mathbf{curl};\Omega)$, for $\mathbf{L}$ the norm of $\mathbf{H}(\mathrm{div};\Omega)$ etc.

Remark 1.2. In order to define precisely the traces on the boundary, we refer the reader to [38].

With the help of Weber (cf. [52]) and Poincaré inequalities, it is possible to define norms for those spaces, which are actually equivalent to the natural norms. These equivalent norms are obtained by removing the L^2-part of the natural norm. For instance, one can prove that the mapping

$$\mathbf{u} \to (\|\mathrm{div}\,\mathbf{u}\|_0^2 + \|\mathbf{curl}\,\mathbf{u}\|_0^2)^{1/2}$$

defines a norm on $\mathbf{X}$, and furthermore that it is equivalent to the norm of $\mathbf{X}$

$$\mathbf{u} \to (\|\mathbf{u}\|_0^2 + \|\mathrm{div}\,\mathbf{u}\|_0^2 + \|\mathbf{curl}\,\mathbf{u}\|_0^2)^{1/2}.$$

It is denoted respectively by $\|\cdot\|_{\mathbf{X}}$. One can proceed similarly for the others spaces (cf. [36]). So, Ψ is equipped with the equivalent norm $\mu \to \|\Delta\mu\|_0$, denoted by $\|\cdot\|_\Psi$.

In what follows, unless otherwise stated, the functional spaces are equipped with the equivalent norms. As far as scalar products are concerned, we use the notation $(\cdot,\cdot)_0$ for the usual one in $L^2(\Omega)$ or $\mathbf{L}^2(\Omega)$, so that the scalar product in $\mathbf{X}$ is $(\cdot,\cdot)_{\mathbf{X}} = (\mathbf{curl}\cdot,\mathbf{curl}\cdot)_0 + (\mathrm{div}\cdot,\mathrm{div}\cdot)_0$, and the scalar product in Ψ is $(\cdot,\cdot)_\Psi = (\Delta\cdot,\Delta\cdot)_0$.

1.2.1. Helmholtz decompositions and mappings

The *singular complement method* is based on mappings, which allow to link electromagnetic fields to:

- on the one hand, scalar or vector potentials, called *primal* fields;
- on the other hand, elements of the range of the Laplace operator, called *dual* fields.

One uses first a Helmholtz decomposition, to split the space of electromagnetic fields into two parts: a subspace of divergence-free fields, and a subspace of curl-free fields.

Theorem 1.3. *The following direct, and orthogonal, Helmholtz decomposition holds*:

$$\mathbf{X} = \mathbf{V} \overset{\perp_{\mathbf{X}}}{\oplus} \mathbf{L}.$$

Second, one defines one-to-one, and onto, mappings, to link the electromagnetic subspaces to the primal or dual spaces of the scalar or vector Laplace operator. We summarize the results in the graphs below (see [36] for details).

In general, results concerning the divergence operator are valid in 2D and 3D. One has

$$\begin{array}{ccccc} & & \xrightarrow{\Delta=\mathrm{div}\,\nabla} & & \\ (\Psi;\|\cdot\|_\Psi) & & & & (L^2(\Omega);\|\cdot\|_0) \\ & \xrightarrow{\nabla} & (\mathbf{L};\|\cdot\|_{\mathbf{L}}) & \xrightarrow{\mathrm{div}} & \end{array}$$

As far as the curl operator is concerned, we refer the reader to [9] for the 2D case. In 3D, the single curl operator is linked to the vector Laplace operator by the relation $\Delta\mathbf{u} = -\,\mathbf{curlcurl}\mathbf{u} + \nabla\mathrm{div}\mathbf{u}$. So, the primal and dual fields are vector fields in 3D. In order to characterize them, one has to choose a gauge condition. This can be achieved by introducing the functional spaces of primal fields

$$\mathbf{\Phi} = \{\boldsymbol{\phi} \in \mathbf{H}(\mathbf{curl},\Omega) : \mathrm{div}\boldsymbol{\phi} = 0,\ \Delta\boldsymbol{\phi} \in \mathbf{L}^2(\Omega),$$
$$\boldsymbol{\phi}\cdot\mathbf{n}_{|_\Gamma} = 0,\ (\mathbf{curl}\boldsymbol{\phi})\times\mathbf{n}_{|_\Gamma} = 0\}.$$

Since the gauge condition amounts to choosing divergence-free primal fields, the vector Laplace operator reduces to $\Delta\mathbf{u} = -\mathbf{curlcurl}\mathbf{u}$, for all primal fields $\mathbf{u}$. The functional space of dual fields is in this case

$$\mathbf{H}_0(\mathrm{div}\,0;\Omega) = \{\mathbf{u} \in \mathbf{L}^2(\Omega),\ \mathrm{div}\,\mathbf{u} = 0;\ \mathbf{u}\cdot\mathbf{n}_{|_\Gamma} = 0\}.$$

One gets finally the graph

$$\begin{array}{ccccc} & & \xrightarrow{\Delta=-\mathrm{curl}\,\mathrm{curl}} & & \\ (\mathbf{\Phi};\|\cdot\|_{\mathbf{\Phi}}) & & & & (\mathbf{H}_0(\mathrm{div}\,0;\Omega);\|\cdot\|_0) \\ & \xrightarrow{\mathbf{curl}} & (\mathbf{V};\|\cdot\|_{\mathbf{V}}) & \xrightarrow{\mathbf{curl}} & \end{array}$$

Now, one can rewrite the Helmholtz decompositions of the space $\mathbf{X}$ to reach in 3D

$$\mathbf{X} = \mathbf{curl}\Phi \overset{\perp_{\mathbf{X}}}{\oplus} \nabla\Psi.$$

With the help of these results, it is now possible to derive splittings of the space of electromagnetic fields into a two-part, direct, sum: a subspace of regular fields, and a subspace of singular fields.

1.2.2. Regular/singular splittings

When the domain is convex, the space of electric fields $\mathbf{X}$, and its subspaces, are included in $\mathbf{H}^1(\Omega)$. Correspondingly, the primal, scalar spaces Ψ is included in $H^2(\Omega)$, and the primal, vector space $\mathbf{\Phi}$ is included in

$$\mathbf{H}^1(\mathbf{curl},\Omega) = \{\mathbf{u} \in \mathbf{H}^1(\Omega), \mathbf{curl}\,\mathbf{u} \in \mathbf{H}^1(\Omega)\}.$$

That is not the case anymore in a 2D, polygonal, non-convex domain (see for instance [40]). Nevertheless, one introduces the regular subspaces for electromagnetic fields (indexed with R)

$$\mathbf{X}_{\mathrm{R}} = \mathbf{X} \cap \mathbf{H}^1(\Omega), \quad \mathbf{V}_{\mathrm{R}} = \mathbf{V} \cap \mathbf{H}^1(\Omega), \quad \mathbf{L}_{\mathrm{R}} = \mathbf{L} \cap \mathbf{H}^1(\Omega).$$

For the primal, scalar, fields, one proceeds similarly

$$\Psi_R = \Psi \cap H^2(\Omega).$$

Remark 1.4. In 3D, the situation is not so straightforward for the primal, vector, fields, by considering the intersection with the space $\mathbf{H}^1(\mathbf{curl}, \Omega)$. As a matter of fact, one cannot guarantee that the inverse image $\boldsymbol{\phi} \in \boldsymbol{\Phi}$ of an element of $\mathbf{v}_R \in \mathbf{V}_R$ belongs to $\mathbf{H}^1(\Omega)$. To address this difficulty, one can nevertheless consider the regular subspace below:

$$\boldsymbol{\Phi}_R = \{\boldsymbol{\phi}_R \in \boldsymbol{\Phi}; \mathbf{curl}\boldsymbol{\phi}_R \in \mathbf{V}_R\}.$$

Each regular subspace is actually closed in its space (proofs can be found in [36]), so that one is able to consider the orthogonal subspace, and then define a two-part, direct, and orthogonal sum of the space. The orthogonal subspaces are called singular subspaces (indexed with S). The orthogonality condition is understood in the sense of the scalar products of the equivalent norms. For the primal, scalar, fields, one has

$$\Psi = \Psi_R \overset{\perp_\Psi}{\oplus} \Psi_S.$$

Whereas, for the electric field, one can write

$$\mathbf{X} = \mathbf{X}_R \overset{\perp_X}{\oplus} \mathbf{X}_S, \quad \mathbf{V} = \mathbf{V}_R \overset{\perp_V}{\oplus} \mathbf{V}_S, \quad \mathbf{L} = \mathbf{L}_R \overset{\perp_L}{\oplus} \mathbf{L}_S.$$

The same property can be proven, for the spaces of dual fields. The subspace $\Delta\Psi_R$ is closed in $L^2(\Omega)$, so one can define the dual singular subspaces by orthogonality. Let S_D denote the singular subspace, associated to the range of the scalar Laplace operator, with homogeneous Dirichlet boundary condition. Similarly, let $\mathbf{S}_0$ denote the orthogonal subspace of $\Delta\boldsymbol{\Phi}_R$ in $\mathbf{H}_0(\mathrm{div}\,0;\Omega)$. These dual singular subspaces can be characterized by (cf. [40] in 2D, or [2,36,4] in 3D)

$$S_D = \{s_d \in L^2(\Omega); \Delta s_d = 0 \text{ in } \Omega, s_{d|\Gamma} = 0\}, \tag{2}$$

$$\mathbf{S}_0 = \left\{\mathbf{s}_0 \in \mathbf{H}_0(\mathrm{div}\,0;\Omega); \Delta\mathbf{s}_0 = 0 \text{ in } \Omega, \left(\frac{\partial \mathbf{s}_0}{\partial \mathbf{n}}\right) \times \mathbf{n}_{|\Gamma} = 0\right\}. \tag{3}$$

In the above definitions, the traces on the boundary are understood in a very weak sense, and in general it is meaningful not on Γ as a whole, but face by face only. One gets the orthogonal decompositions of the dual spaces

$$L^2(\Omega) = \Delta\Psi_R \overset{\perp_0}{\oplus} S_D, \quad \mathbf{H}_0(\mathrm{div}\,0;\Omega) = \Delta\boldsymbol{\Phi}_R \overset{\perp_0}{\oplus} \mathbf{S}_0.$$

Thus, one can split an element $\mathbf{u}$ of one of those spaces into an orthogonal sum of a *regular* part and of a *singular* part: $\mathbf{u} = \mathbf{u}_R + \mathbf{u}_S$. Evidently, all mappings are valid when considered on the regular or singular subspaces (see [36]).

Let us conclude this preliminary study by a result, which is very important as far as numerical computations are concerned. As a matter of fact, one can also introduce direct, but non-orthogonal, two-part sums of the space $\mathbf{X}$. Following [18,36], one can prove

$$\mathbf{X} = \mathbf{X}_R \oplus \mathbf{V}_S, \quad \mathbf{X} = \mathbf{X}_R \oplus \mathbf{L}_S.$$

In this light, $\mathbf{X}_S$ appears as the orthogonal projection of $\mathbf{V}_S$ or $\mathbf{L}_S$ in $\mathbf{X}$, with respect to $\mathbf{X}_R$. A comparative study of the orthogonal decomposition, and of the two non-orthogonal decompositions of $\mathbf{X}$, is carried out in Section 3.

1.3. Characterizations of singular electromagnetic fields

Let us characterize the singular electromagnetic fields, using the results on the dual singular subspaces, recalled at (2) and (3). Following [36], elements $\mathbf{x}_S \in \mathbf{X}_S$ and curl-free elements $\mathbf{l}_S \in \mathbf{L}_S$ respectively satisfy

$$\Delta\mathbf{x}_S = 0 \quad \text{in } \Omega, \quad \mathrm{div}\,\mathbf{l}_S \in S_D \quad \text{in } \Omega,$$
$$\mathbf{x}_S \times \mathbf{n}_{|\Gamma} = 0, \quad \mathbf{l}_S \times \mathbf{n}_{|\Gamma} = 0.$$

We do not present characterizations of singular subspaces made of divergence-free elements here, since we are interested in non-divergence-free solutions. Let us briefly recall that one has to consider separately the 2D and 3D cases. In the 2D case, one fundamentally uses the connections between the gradient and vector curl operators (cf. [9,36]). On the contrary, in 3D, one has to proceed differently. One gets for instance [7]

$$\mathbf{curl}\,\mathbf{curl}\,\mathbf{V}_S \subset \nabla S_D,$$

which is not very useful numerically. Under these conditions, a non-orthogonal sum like $\mathbf{X} = \mathbf{X}_R \oplus \mathbf{L}_S$ is all the more interesting in 3D (see [36] for a numerical illustration, concerning the electromagnetic generated around the tip of a cone).

Remark 1.5. According to the Helmholtz decomposition of $\mathbf{X}$, and to the regular/singular splittings of $\mathbf{L}$ and $\mathbf{V}$, one notices that

$$\mathbf{X} = (\mathbf{L}_R \overset{\perp_X}{\oplus} \mathbf{L}_S) \overset{\perp_X}{\oplus} (\mathbf{V}_R \overset{\perp_X}{\oplus} \mathbf{V}_S) = \mathbf{X}_R \overset{\perp_X}{\oplus} \mathbf{X}_S.$$

Since both $\mathbf{L}_R$ and $\mathbf{V}_R$ are closed subspaces of $\mathbf{X}_R$, one infers that $(\mathbf{L}_R \overset{\perp_X}{\oplus} \mathbf{V}_R) \subset \mathbf{X}_R$, and also that $\mathbf{X}_S \subset (\mathbf{L}_S \overset{\perp_X}{\oplus} \mathbf{V}_S)$. A priori, one might think that the reverse inclusions hold, which is incorrect. For instance, in 2D, and can prove the result

$$\dim(\mathbf{X}_S) = \dim(\mathbf{L}_S) = \dim(\mathbf{V}_S).$$

What happens is that elements of $\mathbf{L}_S$, $\mathbf{V}_S$ and $\mathbf{X}_S$ have the same principal part, up to a (multiplicative) constant (cf. Section 3.1).

1.4. Incoming plane waves

Now, let us consider that the boundary Γ is made up of two parts: Γ_C and Γ_A, with Γ_C the *perfect conducting boundary*, and Γ_A an *artificial boundary*. We further split the artificial boundary Γ_A into Γ_A^i and Γ_A^a. On Γ_A^i, we model incoming plane waves, whereas we impose on Γ_A^a an absorbing boundary condition. One has

$$(\mathscr{E} - c\mathscr{B} \times \mathbf{n}) \times \mathbf{n} = \mathbf{e}^{\star} \times \mathbf{n} \quad \text{on } \Gamma_A, \tag{4}$$

or, equivalently,

$$(c\mathscr{B} + \mathscr{E} \times \mathbf{n}) \times \mathbf{n} = c\mathbf{b}^{\star} \times \mathbf{n} \quad \text{on } \Gamma_A. \tag{5}$$

The surface fields $\mathbf{e}^{\star}$ and $\mathbf{b}^{\star}$ are data. They either define the characteristics of the incoming plane waves on Γ_A^i, or vanish on Γ_A^a. On Γ_A^i, these surface fields are always *regular*, in the sense that they are the traces of smooth (in the sense of [20]), incident, fields. On Γ_A^a, this boundary condition – often called Silver–Müller boundary condition [49] – is a first order absorbing boundary condition.

Without loss of generality, one can choose the location of the artificial boundary Γ_A, so that it does not intersect with a geometrical singularity. What is more, one can also choose a regular shape for Γ_A, which means that there is no geometrical singularity in Γ_A. In this way, the electromagnetic field is *regular* in a 3D neighborhood of the artificial boundary, called Ω_A. Indeed, outside the perfect conducting body, the electromagnetic field is strong only in the neighborhood of geometrical singularities.

How[1] can this be expressed mathematically? Let us split the electric field like

$$\mathscr{E} = \eta_A \mathscr{E} + (1 - \eta_A)\mathscr{E} \quad \text{in } \Omega,$$

where η_A is a smooth truncation function, which vanishes outside of Ω_A, and which is equal to one in a 3D neighborhood of Γ_A, called ω_A ($\omega_A \subset \Omega_A$). By construction, there holds

$$\eta_A \mathscr{E} \in \mathbf{H}^1(\Omega) \quad \text{and} \quad (1 - \eta_A)\mathscr{E} \in \mathbf{X}.$$

A priori, one has $\eta_A \mathscr{E}_{|\Gamma_A} \neq 0$ (whereas $\eta_A \mathscr{E}_{|\Gamma_C} = 0$, since $\mathscr{E}$ satisfies the perfect conducting boundary condition on Γ_C). In other words, one can split the electric field as a two-term sum: the first one belongs to $\mathbf{X}$, and the second one belongs to $\mathbf{X}_R^{\Gamma_A}$, where $\mathbf{X}_R^{\Gamma_A}$ is the subspace of regular electric fields defined by

$$\mathbf{X}_R^{\Gamma_A} = \{\mathbf{v} \in \mathbf{H}^1(\Omega) : \mathbf{v} \times \mathbf{n}_{|\Gamma_C} = 0\}.$$

Last, if one denotes by $\underline{\mathbf{X}}$ the space of all possible electric fields, one concludes that

$$\underline{\mathbf{X}} = \mathbf{X}_R^{\Gamma_A} + \mathbf{X} = \mathbf{X}_R^{\Gamma_A} + (\mathbf{X}_R \oplus \mathbf{X}_S) = \mathbf{X}_R^{\Gamma_A} \oplus \mathbf{X}_S,$$

since one has by definition $\mathbf{X}_R \subset \mathbf{X}_R^{\Gamma_A}$.

Numerically, this splitting is interesting. On the one hand, the subspace of singular electric fields is $\mathbf{X}_S$, as before (it could also be $\mathbf{L}_S$, or $\mathbf{V}_S$). Thus, modelling incoming plane waves, or imposing an absorbing boundary condition as no impact, as far as the singular subspace is concerned. On the other hand, as soon as Γ_A^i is not empty, one has to add, in the variational formulation, terms on Γ_A^i. But, since elements of $\mathbf{X}_S$ have a vanishing tangential trace, no singular term has to be added.

[1] Due to the locality of the geometrical singularities, one may think that non-standard boundary condition imposed on a regular part of the boundary can be treated easily. Unfortunately, as proved in [31], the effect of geometrical singularities is non-local (i.e. they influence the solution in the whole domain) and this problem must be investigated.

2. Numerical algorithms and error analysis

It is now possible to build numerical algorithms, based on the results of the previous section. We call them *singular complement methods*, or *SCM*. The general framework of an *SCM* is sketched below:

1. Choose the best suited splitting into regular and singular subspaces.
2. Compute numerically an approximation of the basis of the singular subspace. Since this computation is independent of the time variable, it is achieved at the initialization stage.
3. Solve the problem by coupling a classical method, which relies for instance on a continuous finite element approximation and allows to compute the regular part of the solution, to the linear system, which allows to compute the singular part of the solution. In the case of finite dimensional singular subspaces, this linear system possesses exactly the dimension of this subspace. In general, the dimension is small, so one computes explicitly the inverse of the matrix at the initialization stage.

Let $\mathbf{U}$ denote one of the spaces of electromagnetics fields $\mathbf{X}$, $\mathbf{V}$, etc. One knows from the regular/singular splittings that $\mathbf{U}_R$ is not dense in $\mathbf{U}$, as soon as its orthogonal $\mathbf{U}_S$ is not reduced to $\{0\}$. Let $\mathbf{u} = \mathbf{u}_R + \mathbf{u}_S$ be the solution we seek to approximate. If $\mathbf{u}^h$ denotes the discrete solution, obtained by a continuous approximation, and *conforming* in $\mathbf{U}$, one has $\mathbf{u}^h \in \mathbf{U} \cap \mathbf{H}^1(\Omega) = \mathbf{U}_R$. Therefore, one finds

$$\|\mathbf{u} - \mathbf{u}^h\|_{\mathbf{U}}^2 = \|\mathbf{u}_R - \mathbf{u}^h\|_{\mathbf{U}}^2 + \|\mathbf{u}_S\|_{\mathbf{U}}^2 \geqslant \|\mathbf{u}_S\|_{\mathbf{U}}^2.$$

In other words, as soon as $\mathbf{U}_S$ is not reduced to $\{0\}$, a conforming, continuous approximation fails to converge to the true solution when h goes to 0. In particular, mesh refinement techniques fail too! The idea behind the *SCM* is to introduce a – conforming – approximation of the singular part, which we denote by $\mathbf{u}_S^h$, so that one has

$$\|\mathbf{u} - (\mathbf{u}^h + \mathbf{u}_S^h)\|_{\mathbf{U}}^2 = \|\mathbf{u}_R - \mathbf{u}^h\|_{\mathbf{U}}^2 + \|\mathbf{u}_S - \mathbf{u}_S^h\|_{\mathbf{U}}^2.$$

Thus, the aim is to find a "good" approximation technique for the singular part of the solution, and also for the regular part of the solution, so that $\mathbf{u}_S^h \to \mathbf{u}_S$ and $\mathbf{u}^h \to \mathbf{u}_R$.

Remark 2.1. One achieves convergence with $\mathbf{u}^h$ only, when the solution $\mathbf{u}$ is itself smooth, i.e. $\mathbf{u} \in \mathbf{U}_R$. Unfortunately, from a statistical point of view, this situation does not occur in practice. However, the situation is different for eigenvalue problems [31]: some electromagnetic eigenmodes are smooth, and they do belong to $\mathbf{U}_R$.

2.1. Computation of the singular bases

There exist several methods, to compute the singular basis functions (Dirichlet-to-Neumann techniques [9,8], use of a truncation function [47,43], etc.). We recall here

briefly the method we choose, the *principal part method*. We refer the reader to [6] for a detailed presentation. The prerequisite, for using this method, is that the *principal part* – the most singular part – of the primal and dual singular fields in the neighborhood of the geometrical singularities, must be known explicitly. In general, this is fairly straightforward for finite dimensional singular subspaces.

Consider, for simplicity reasons, a domain such that the singular subspace is of dimension one. For instance, a 2D domain with a single reentrant corner, or a 3D domain with a single sharp conical vertex [39,6]. Let $s_{\mathrm{N}}^{\mathrm{P}}$ (respectively $s_{\mathrm{D}}^{\mathrm{P}}$) denote the principal part of the dual singular fields, which belongs to the range of the scalar Laplace operator, with homogeneous Neumann (respectively Dirichlet) boundary condition.

The PPM consists in the following splitting of dual singular functions:

$$s_{\mathrm{N}} = s_{\mathrm{N}}^{\mathrm{P}} + \tilde{s}_{\mathrm{N}}, \quad s_{\mathrm{D}} = s_{\mathrm{D}}^{\mathrm{P}} + \tilde{s}_{\mathrm{D}}. \tag{6}$$

Above, $\tilde{s}_{\mathrm{N}}$ and $\tilde{s}_{\mathrm{D}}$ belong to $H^1(\Omega)$. The principal parts $s_{\mathrm{N}}^{\mathrm{P}}$ and $s_{\mathrm{D}}^{\mathrm{P}}$ – which belong to $L^2(\Omega)$ but not to $H^1(\Omega)$ – are harmonic. In addition, their trace on the boundary fulfills *locally*, that is in the neighborhood of the geometrical singularity, the homogeneous Neumann or Dirichlet boundary condition.

One computes, for instance by a P^1 finite element method (see Section 2.4), the parts $\tilde{s}_{\mathrm{N}}$ and $\tilde{s}_{\mathrm{D}}$ by solving – in $H^1(\Omega)$ – for $\tilde{s}_{\mathrm{N}}$

$$\text{Find } \tilde{s}_{\mathrm{N}} \in H^1(\Omega) \cap L_0^2(\Omega) \text{ such that } \Delta \tilde{s}_{\mathrm{N}} = 0 \text{ in } \Omega,$$
$$\frac{\partial \tilde{s}_{\mathrm{N}}}{\partial \boldsymbol{\nu}} = -\frac{\partial s_{\mathrm{N}}^{\mathrm{P}}}{\partial \boldsymbol{\nu}} \quad \text{on } \Gamma, \tag{7}$$

and for $\tilde{s}_{\mathrm{D}}$

$$\text{Find } \tilde{s}_{\mathrm{D}} \in H^1(\Omega) \text{ such that } \Delta \tilde{s}_{\mathrm{D}} = 0 \text{ in } \Omega, \quad \tilde{s}_{\mathrm{D}} = -s_{\mathrm{D}}^{\mathrm{P}} \text{ on } \Gamma. \tag{8}$$

In this way, it is possible to compute approximations of the dual singular basis functions, without mesh refinement techniques [48,25].

One then uses the singular mappings, to find the primal singular fields

$$\text{Find } \phi_{\mathrm{S}} \in H^1(\Omega) \cap L_0^2(\Omega) \text{ such that } -\Delta \phi_{\mathrm{S}} = s_{\mathrm{N}} \text{ in } \Omega,$$
$$\frac{\partial \phi_{\mathrm{S}}}{\partial \boldsymbol{\nu}} = 0 \text{ on } \Gamma, \tag{9}$$

$$\text{Find } \psi_{\mathrm{S}} \in H^1(\Omega) \text{ such that } -\Delta \psi_{\mathrm{S}} = s_{\mathrm{D}} \text{ in } \Omega,$$
$$\psi_{\mathrm{S}} = 0 \text{ on } \Gamma. \tag{10}$$

One can split the primal fields like

$$\phi_{\mathrm{S}} = \tilde{\phi}_{\mathrm{S}} + C_\phi \phi_{\mathrm{S}}^{\mathrm{P}}, \tag{11}$$

$$\psi_{\mathrm{S}} = \tilde{\psi}_{\mathrm{S}} + C_\psi \psi_{\mathrm{S}}^{\mathrm{P}}. \tag{12}$$

Above, $\tilde{\phi}_{\mathrm{S}}$ and $\tilde{\psi}_{\mathrm{S}}$ belong to $H^2(\Omega)$, and C_ϕ and C_ψ are two constants, to be determined. The principal parts $\phi_{\mathrm{S}}^{\mathrm{P}}$ and $\psi_{\mathrm{S}}^{\mathrm{P}}$ are harmonic – do not belong to $H^2(\Omega)$ – and fulfill locally the ad hoc boundary condition. Their analytic expression is known. The computation of the constants C_ϕ and C_ψ is presented in the next Subsection. The regular parts $\tilde{\phi}_{\mathrm{S}}$ and $\tilde{\psi}_{\mathrm{S}}$ can be computed easily, by solving a standard variational formulation (see Section 2.4).

Then, using the singular mappings, one can compute the singular electromagnetic basis functions. To determine the basis $\mathbf{v}_{\mathrm{S}}$ (respectively $\mathbf{l}_{\mathrm{S}}$) of $\mathbf{V}_{\mathrm{S}}$ (respectively $\mathbf{L}_{\mathrm{S}}$), one simply takes the curl of ϕ_{S} (respectively the gradient of ψ_{S}). It is written

$$\mathbf{v}_{\mathrm{S}} = \mathbf{curl}\tilde{\phi}_{\mathrm{S}} + C_\phi \mathbf{curl}\phi_{\mathrm{S}}^{\mathrm{P}}, \tag{13}$$

$$\mathbf{l}_{\mathrm{S}} = \nabla \tilde{\psi}_{\mathrm{S}} + C_\psi \nabla \psi_{\mathrm{S}}^{\mathrm{P}}. \tag{14}$$

The principal parts are $C_\phi \mathbf{curl}\phi_{\mathrm{S}}^{\mathrm{P}}$ and $C_\psi \nabla \psi_{\mathrm{S}}^{\mathrm{P}}$, and the regular parts are $\mathbf{curl}\tilde{\phi}_{\mathrm{S}}$ and $\nabla \tilde{\psi}_{\mathrm{S}}$.

2.2. Singular constants

In (6), the principal part is equal to $1 \times s_{\mathrm{D}}^{\mathrm{P}}$ or $1 \times s_{\mathrm{N}}^{\mathrm{P}}$. One could choose other values, up to a non-zero multiplicative constant. Anyway, the principal part determines the regularity of the dual singular fields, which is non-smooth only at reentrant corners, as proved by Grisvard in [40].

Then, setting the constants to one in (6) prescribes the values of the other constants, for instance of C_ϕ in (11), since singular fields are related to one another by one-to-one mappings. Let us investigate now, how one can obtain formulas to compute those constants. A possibility is to use an integral equality, based on an integration by parts. This type of formula is labeled "stress intensity factor" in mechanics. For instance, for C_ϕ, one can integrate by parts – with caution, see [2,4] – to reach

$$\int_\Omega p \Delta \varphi \, \mathrm{d}\Omega - \int_\Omega \varphi \Delta p \, \mathrm{d}\Omega = \text{“} \int_\Gamma p \frac{\partial \varphi}{\partial \boldsymbol{\nu}} \mathrm{d}\Gamma - \int_\Gamma \varphi \frac{\partial p}{\partial \boldsymbol{\nu}} \mathrm{d}\Gamma \text{”}.$$

Choosing $p = s_{\mathrm{N}}$ and $\varphi = \tilde{\phi}_{\mathrm{S}} = \phi_{\mathrm{S}} - C_\phi \phi_{\mathrm{S}}^{\mathrm{P}}$, one gets

$$C_\phi = \frac{\|s_{\mathrm{N}}\|^2}{\displaystyle\int_\Gamma s_{\mathrm{N}} \frac{\partial \phi_{\mathrm{S}}^{\mathrm{P}}}{\partial \boldsymbol{\nu}} \mathrm{d}\Gamma}. \tag{15}$$

An alternative is proved below, for the constant C_ψ of (12). To that aim, one defines a neighborhood $\mathscr{V}_\varepsilon$ of the geometrical singularity by taking the intersection of the domain Ω with the ball of radius $\varepsilon > 0$ centered at the geometrical singularity. Define $\Omega_\varepsilon = \Omega \setminus \mathscr{V}_\epsilon$ and $\Gamma_\varepsilon = \partial\Omega_\varepsilon \backslash \partial\Gamma$. There holds

Proposition 2.2. *The constant C_ψ can be expressed as*

$$C_\psi = \frac{\|s_{\mathrm{D}}\|^2}{\lim_{\varepsilon\to 0} \displaystyle\int_{\Gamma_\varepsilon} \frac{\partial s_{\mathrm{D}}^{\mathrm{P}}}{\partial \mathbf{n}_\varepsilon}(\psi_{\mathrm{S}}^{\mathrm{P}}) \, \mathrm{d}\Gamma - \lim_{\varepsilon\to 0} \displaystyle\int_{\Gamma_\varepsilon} \frac{\partial(\psi_{\mathrm{S}}^{\mathrm{P}})}{\partial \mathbf{n}_\varepsilon} s_{\mathrm{D}}^{\mathrm{P}} \, \mathrm{d}\Gamma}.$$

Proof. Following [50], one knows that $\psi_{\mathrm{S}}^{\mathrm{P}}$ belongs to $H^2(\Omega_\varepsilon)$.

Let η be a truncation function defined on $\mathbb{R}^+$, equal to one in a neighborhood of zero, and to zero in $[1, +\infty[$. Split ψ_{S} as

$$\psi_{\mathrm{S}} = \tilde{\psi}_{\mathrm{S}} + C_\psi(1-\eta)\psi_{\mathrm{S}}^{\mathrm{P}} + C_\psi \eta \psi_{\mathrm{S}}^{\mathrm{P}}.$$

Since $(\eta\psi_S^P)_{|\Gamma} = 0$, it is clear that $\tilde{\psi}_S + C_\psi(1-\eta)\psi_S^P \in \Psi_R$. Then, using the orthogonality in Ψ, and the relation between primal and dual singular functions $\Delta\psi_S = -s_D$, one gets

$$\|s_D\|_0^2 = -\int_\Omega \Delta\psi_S s_D \,d\Omega = -C_\psi \int_\Omega \Delta(\eta\psi_S^P) s_D \,d\Omega.$$

The right-hand side integral can be split as

$$\int_\Omega \Delta(\eta\psi_S^P) s_D \,d\Omega = \int_\Omega \Delta(\eta\psi_S^P)\tilde{s}_D \,d\Omega + \int_\Omega \Delta(\eta\psi_S^P) s_D^P \,d\Omega.$$

The first term of the right-hand side vanishes after standard integration by parts

$$\int_\Omega \Delta(\eta\psi_S^P)\tilde{s}_D \,d\Omega = \int_\Omega (\eta\psi_S^P)\Delta\tilde{s}_D \,d\Omega + \int_\Gamma \tilde{s}_D \frac{\partial(\eta\psi_S^P)}{\partial \boldsymbol{\nu}} d\Gamma - \int_\Gamma (\eta\psi_S^P)\frac{\partial\tilde{s}_D}{\partial \boldsymbol{\nu}} d\Gamma.$$

As a matter of fact, one has $\Delta\tilde{s}_D = 0$ in Ω. Then, $\tilde{s}_{D|\Gamma}$ vanishes around the geometrical singularity, whereas $\partial_\nu(\eta\psi_S^P)_{|\Gamma}$ vanishes on the remainder of the boundary. Finally, $(\eta\psi_S^P)_{|\Gamma} = 0$.

Standard integration by parts is not possible anymore for the second term. So, one rewrites it as a limit, when ε goes to zero,

$$\int_\Omega \Delta(\eta\psi_S^P) s_D^P \,d\Omega = \lim_{\varepsilon\to 0} \int_{\Omega_\varepsilon} \Delta(\eta\psi_S^P) s_D^P \,d\Omega.$$

In Ω_ε, the principal parts are sufficiently smooth, so that one can use the usual integration by parts formulas, to reach

$$\int_\Omega \Delta(\eta\psi_S^P) s_D^P \,d\Omega = -\lim_{\varepsilon\to 0} \int_{\Gamma_\varepsilon} \frac{\partial s_D^P}{\partial \mathbf{n}_\varepsilon}(\eta\psi_S^P)\,d\Gamma + \lim_{\varepsilon\to 0} \int_{\Gamma_\varepsilon} \frac{\partial(\eta\psi_S^P)}{\partial \mathbf{n}_\varepsilon} s_D^P \,d\Gamma.$$

Then, for sufficiently small ε, $\eta(\mathbf{z}) = 1$ for all $\mathbf{z} \in \Gamma_\varepsilon$, and the result follows. □

In practice, one uses this formula by plugging the explicit dependence of the trace of the normal derivative on Γ_ε, with respect to the coordinates. For instance, in the local polar or spherical coordinates, there holds $\partial_{\mathbf{n}_\varepsilon} = -\partial_r$. An example is given in Section 2.5.

Remark 2.3. To compute the singular electromagnetic basis fields, one does not have to compute additional multiplicative constants, since these fields are obtained directly by differentiating (14).

2.3. Variational formulations and their discretizations

In this section, we recall some *variational formulations*, or *VF*, which have been developed to solve the instationary problem. We also introduce the discretization of these VFs.

Ampère's and Faraday's laws can be written equivalently as two second-order in time equations, plus suitable initial and boundary conditions. In this form, the electric and magnetic fields are decoupled (up to the initial conditions). For stability reasons (such as the control of the discrete energy [3]), and to minimize the computational cost, we prefer to discretize this set of equations, instead of the first-order Maxwell equations.

What is more, to enforce the divergence constraints on the electromagnetic field, we introduce two Lagrange multipliers. They are used to dualize Coulomb's and absence of free magnetic monopole's laws, which are therefore considered as constraints of the second order in time equations. In this way, one builds a mixed VF of Maxwell equations. It is well posed, as soon as the well-known *inf–sup* (or Babuska–Brezzi [12,19]) condition holds. In addition to begin mixed, we use here augmented VFs , which results in a mixed, augmented VF, or *MAVF*. To this end, one adds to the bilinear form $(\mathbf{curl}\cdot, \mathbf{curl}\cdot)_0$, the term $(\mathrm{div}\cdot, \mathrm{div}\cdot)_0$. In our case, the electric field belongs to $\mathbf{X}$, or to $\underline{\mathbf{X}}$ in the case of incoming plane waves. Then, the correct Lagrange multiplier space is $L^2(\Omega)$. Let $p(t)$ be the Lagrange multiplier.

This MAVF has been developed in 2D (cartesian or axisymmetric geometries) and in 3D (see among others [10]). We present here the case of the electric field, but the case of the magnetic field is handled similarly. One has to include the *SCM* in this formulation. After choosing the most appropriate singular subspace – for instance $\mathbf{X} = \mathbf{X}_R \oplus \mathbf{X}_S$ – the electric field $\mathscr{E}$ is split like

$$\mathscr{E}(t) = \mathscr{E}_R(t) + \mathscr{E}_S(t). \tag{16}$$

(Above, we state explicitly the dependency with respect to time.) The same splitting is used for test-fields. The MAVF reads:

$$\begin{aligned}
&\text{Find } (\mathscr{E}_R(t), \mathscr{E}_S(t), p(t)) \in \mathbf{X}_R \times \mathbf{X}_S \times L^2(\Omega) \text{ such that}\\
&\frac{d^2}{dt^2}(\mathscr{E}_R(t), \mathbf{x}_R)_0 + c^2(\mathscr{E}_R(t), \mathbf{x}_R)_{\mathbf{X}} + (p(t), \mathrm{div}\,\mathbf{x}_R)_0\\
&\quad = -\frac{1}{\varepsilon_0}\frac{d}{dt}(\mathscr{J}(t), \mathbf{x}_R)_0 + \frac{c^2}{\varepsilon_0}(\rho(t), \mathrm{div}\,\mathbf{x}_R)_0\\
&\qquad -\frac{d^2}{dt^2}(\mathscr{E}_S(t), \mathbf{x}_R)_0 - c^2(\mathscr{E}_S(t), \mathbf{x}_R)_{\mathbf{X}} \quad \forall \mathbf{x}_R \in \mathbf{X}_R, \qquad (17)\\
&\frac{d^2}{dt^2}(\mathscr{E}_S(t), \mathbf{x}_S)_0 + c^2(\mathscr{E}_S(t), \mathbf{x}_S)_{\mathbf{X}} + (p(t), \mathrm{div}\,\mathbf{x}_S)_0\\
&\quad = -\frac{1}{\varepsilon_0}\frac{d}{dt}(\mathscr{J}(t), \mathbf{x}_S)_0 + \frac{c^2}{\varepsilon_0}(\rho(t), \mathrm{div}\,\mathbf{x}_S)_0\\
&\qquad -\frac{d^2}{dt^2}(\mathscr{E}_R(t), \mathbf{x}_S)_0 - c^2(\mathscr{E}_R(t), \mathbf{x}_S)_{\mathbf{X}} \quad \forall \mathbf{x}_S \in \mathbf{X}_S, \qquad (18)\\
&(\mathrm{div}\mathscr{E}_R(t), q)_0 + (\mathrm{div}\mathscr{E}_S(t), q)_0 = \frac{1}{\varepsilon_0}(\rho(t), q)_0 \quad \forall q \in L^2(\Omega). \qquad (19)
\end{aligned}$$

Remark 2.4

1. In the case of an orthogonal splitting, one could omit terms like $(\mathscr{E}_S(t), \mathbf{x}_R)_{\mathbf{X}}$, or $(\mathscr{E}_R(t), \mathbf{x}_S)_{\mathbf{X}}$, which vanish. They are kept, in order to present a formulation valid

in all cases. Analogously, one could use a non-orthogonal splitting, with a singular subspace made of divergence-free or curl-free fields – $\mathbf{V}_S$ or $\mathbf{L}_S$ – and therefore omit the corresponding terms.

2. One can write similar formulations in $\mathbf{V} = \mathbf{V}_R \overset{\perp}{\oplus} \mathbf{V}_S$, and in $\mathbf{L} = \mathbf{L}_R \overset{\perp}{\oplus} \mathbf{L}_S$ (see [9,6]).
3. In practice, one can use a slightly modified formulation, which is based on the following formula. Since both $\mathscr{E}_R(t)$ and x_R belong to $\mathbf{H}^1(\Omega)$, it is possible to replace, in (17), the scalar product $(\mathscr{E}_R(t), \mathbf{x}_R)_X$ by (cf. [10])

$$(\mathbf{grad}\,\mathscr{E}_R(t), \mathbf{grad}\,\mathbf{x}_R)_0 + \text{boundary terms}.$$

4. What is added, when compared to the MAVF, posed in a convex domain? First, Eq. (18). Second, additional terms appear in (17) and (19), which express the coupling between singular and regular parts. However, these terms are independent of the time variable, so they are computed once and for all, at the initialization stage.

This MAVF is first discretized in time, with the help of the well-known leap-frog scheme. From a practical point of view, one builds a space-discretized MAVF by choosing discrete fields and test-functions, which fulfill a uniform, discrete *inf–sup* boundary condition, to approximate the regular part of the solution. We choose the Taylor–Hood, P_2-iso-P_1 finite element [24]. In addition to being well-suited for discretizing saddle-point problems, it allows to build diagonal mass matrices, when suitable quadrature formulas are used. Thus, the solution to the linear system, which involves the mass matrix, is straightforward [10].

To discretize the singular part, we assume that either the singular subspace is finite dimensional, or the singular subspace is infinite dimensional, but it can be suitably approximated with the help of a finite dimensional discrete space, as in Section 2.5. In both situations, we write down the discrete singular part as a finite sum. So, let $(\mathbf{x}_S^i)_{i=1,N}$ be a given basis of the discrete singular space, of dimension N. (The superscript h is omitted.) One has

$$\mathscr{E}_S(t) = \sum_{i=1}^{N} \kappa^i(t)\mathbf{x}_S^i, \tag{20}$$

where $(\kappa^i)_{i=1}^N$ are continuous time-dependent functions (cf. [3,37] for details).

This results in a fully discretized MAVF:

$$\mathbb{M}_\Omega \vec{\mathsf{E}}_R^{n+1} + \mathbb{M}_{RS}\vec{\kappa}^{n+1} + \mathbb{L}_\Omega \vec{\mathsf{p}}^{n+1} = \vec{\mathsf{F}}^n, \tag{21}$$

$$\mathbb{M}_{RS}^T \vec{\mathsf{E}}_R^{n+1} + \mathbb{M}_S\vec{\kappa}^{n+1} + \mathbb{L}_S \vec{\mathsf{p}}^{n+1} = \vec{\mathsf{G}}^n, \tag{22}$$

$$\mathbb{L}_\Omega^T \vec{\mathsf{E}}_R^{n+1} + \mathbb{L}_S^T\vec{\kappa}^{n+1} = \vec{\mathsf{H}}^n. \tag{23}$$

Above $\mathbb{M}_\Omega$ denotes the usual mass matrix, and $\mathbb{L}_\Omega$ corresponds to the divergence term involving $\mathbf{x}_R^h$ and $p_h(t)$. Then, $\mathbb{M}_{RS}$ is a rectangular matrix, which is obtained by taking $\mathbf{L}^2$ scalar products between regular and singular basis functions, $\mathbb{M}_S$ is the "singular" mass matrix, and finally, $\mathbb{L}_S$ corresponds to the divergence term involving $\mathbf{x}_S^i$ and $p_h(t)$.

To solve this system, one removes the unknown $\vec{\kappa}^{n+1}$. To that aim, replace Eq. (21) by (21) $-\,\mathbb{M}_{RS}\mathbb{M}_S^{-1}$(22), and Eq. (23) by (23) $-\,\mathbb{L}_S^T\mathbb{M}_S^{-1}$(22). In this modified system, only the unknowns $(\vec{\mathsf{E}}_R^{n+1}, \vec{\mathsf{p}}^{n+1})$ appear. If one lets $\widetilde{\ }$ stand for the modified matrices and right-hand sides, it reads

$$\widetilde{\mathbb{M}}\vec{\mathsf{E}}_R^{n+1} + \widetilde{\mathbb{L}}\vec{\mathsf{p}}^{n+1} = \widetilde{\vec{\mathsf{F}}^n},$$

$$\widetilde{\mathbb{L}}^T\vec{\mathsf{E}}_R^{n+1} - \mathbb{L}_S^T\mathbb{M}_S^{-1}\mathbb{L}_S\vec{\mathsf{p}}^{n+1} = \widetilde{\vec{\mathsf{H}}^n}.$$

Its solution can be computed with the help of a Uzawa-type algorithm (cf. [35]).

When compared to the case of a convex domain, the additional computational effort is twofold. First, one has to compute the solution to a linear system with matrix $\mathbb{M}_S^{-1}$. However, since it is a symmetric positive-definite matrix, and usually a low-dimensional one (often $N = 1$), $\mathbb{M}_S^{-1}$ is easily computed, once and for all. Second, the linear system with matrix $\widetilde{\mathbb{M}} = \mathbb{M}_\Omega - \mathbb{M}_{RS}\mathbb{M}_S^{-1}\mathbb{M}_{RS}^T$. Of help is the formula (see [41] for a thorough study),

$$(\mathbb{A} - \mathbb{U}\mathbb{V}^T)^{-1} = \mathbb{A}^{-1} + \mathbb{A}^{-1}\mathbb{U}(\mathbb{I} - \mathbb{V}^T\mathbb{A}^{-1}\mathbb{U})^{-1}\mathbb{V}^T\mathbb{A}^{-1}.$$

Indeed, in our case, $\mathbb{A} = \mathbb{M}_\Omega$ is a diagonal matrix, thus it is straightforward to invert. One has to compute once and for all the $N \times N$ term $(\mathbb{I} - \mathbb{V}^T\mathbb{A}^{-1}\mathbb{U})^{-1}$.

Finally, one concludes the time-stepping scheme by computing $\vec{\kappa}^{n+1}$ with the help of (22).

2.4. Error estimates

Let us briefly recall some well-known results, on the computation of the primal and dual singular functions [25]. For the solution of the electro- and magneto-static problems, we refer the reader to [3,43,45]. Let us consider a 2D polygonal domain Ω, and call π/α_k the angle at the kth reentrant corner. Set $\alpha = \min_k \alpha_k$ ($\alpha \in]\frac{1}{2}, 1[$). Let us triangulate the domain and assume that $\mathscr{T}^h$ is a shape regular triangulation, with a mesh size h, made of triangles (cf. [21]). In this subsection, C is a non-negative constant, which depends only on Ω. To simplify the notations, we omit the exponent i, which varies from one to N (cf. (20)).

One starts with the approximation of s_N, by $s_N^h = \tilde{s}_N^h + s_N^P$. Here, $\tilde{s}_N^h$ is the continuous, P_1 Lagrange finite element solution to the discretized variational formulation associated to (7), which is conforming in $H^1(\Omega)$. There holds

$$\|s_N - s_N^h\|_0 \leqslant Ch^{2\alpha}.$$

To approximate ϕ_S, one checks that the denominator of (15) is equal to 2π, so that one infers

$$|C_\phi - C_\phi^h| \leqslant Ch^{2\alpha}.$$

Then, one considers the approximation $\phi_S^h = \tilde{\phi}_S^h + C_\phi^h\phi_S^P$. Here, $\tilde{\phi}_S^h$ is the continuous, P_1 Lagrange finite element solution to the discretized variational formulation associated to (9). One reaches

$$\|\phi_S - \phi_S^h\|_1 \leqslant Ch.$$

Remark 2.5. One can use the same techniques, and obtain similar results, for s_D, C_ψ and ψ_S.

As far as the electromagnetic singular fields are concerned, let us begin with the approximation of $\mathbf{v}_S$: $\underline{\mathbf{v}}_S^h = \mathbf{curl}\tilde{\phi}_S^h + C_\phi^h \mathbf{curl}\phi_S^P$ (i.e. the discretized version of (13)). In this way, one builds, for the regular part, a – discontinuous – approximation, made of P_0 Lagrange finite elements, component by component. Then, one applies to this approximation the discrete $\mathbf{L}^2$ projection, on the continuous, P_1 Lagrange finite element space. This provides an approximation of the regular part, conforming in $\mathbf{H}^1(\Omega)$. This results in the discrete field $\mathbf{v}_{S,1}^h$ which is, in practice easier to use than the discontinuous one. One can prove easily the estimate [3]

$$\|\mathbf{v}_S - \mathbf{v}_{S,1}^h\|_0 \leqslant Ch.$$

However, one can prefer another approach, previously described in [43]. It yields the following estimate:

$$\forall \varepsilon > 0, \exists C_\varepsilon, \quad \|\mathbf{v}_S - \mathbf{v}_{S,2}^h\|_{\mathbf{X}} \leqslant C_\varepsilon h^{2\alpha-1-\varepsilon} \quad \text{and} \quad \|\mathbf{v}_S - \mathbf{v}_{S,2}^h\|_0 \leqslant C_\varepsilon h^{4\alpha-2-\varepsilon}. \tag{24}$$

With this approach, it is possible to control the whole norm in $\mathbf{X}$, but the exponent depends on the maximal reentrant angle, through the value of α.

Remark 2.6. One can reach similar results for $\mathbf{l}_S$.

Then, by mixing those two approaches [45], one can obtain an error estimate for the basis of $\mathbf{X}_S$, under the form

$$\forall \varepsilon > 0, \exists C_\varepsilon, \quad \|\mathbf{x}_S - \mathbf{x}_S^h\|_{\mathbf{X}} \leqslant C_\varepsilon h^{2\alpha-1-\varepsilon} \quad \text{and} \quad \|\mathbf{x}_S - \mathbf{x}_S^h\|_0 \leqslant C_\varepsilon h^{4\alpha-2-\varepsilon}. \tag{25}$$

Once more, the result depends crucially on α.

As a conclusion, we recall some results, which concern the quality of the effective approximation of the solution, here the electric field. Its regular part is approximated by continuous, P_1 Lagrange finite elements, and is conforming in $\mathbf{H}^1(\Omega)$. More precisely, following (16), one has

$$\mathscr{E}^h = \mathscr{E}_R^h + \sum_{i=1}^{N} \kappa^{i,h} \mathbf{x}_S^{i,h}.$$

Above, the singular part is assumed to belong to $\mathbf{X}_S$ (see (20)). Following [45], one proves

$$1 \leqslant i \leqslant N, \quad |\kappa^i - \kappa^{i,h}| \leqslant Ch^{2\alpha}, \quad \forall \varepsilon > 0, \exists C_\varepsilon, \quad \|\mathscr{E} - \mathscr{E}^h\|_{\mathbf{X}} \leqslant C_\varepsilon h^{2\alpha-1-\varepsilon} \quad \text{and} \quad \|\mathscr{E} - \mathscr{E}^h\|_0 \leqslant C_\varepsilon h^{4\alpha-2-\varepsilon}. \tag{26}$$

For the last line of (26), it is required that the right-hand sides belong to $H^{2\alpha-1-\varepsilon}(\Omega)$. Then, one can prove extra-regularity results for $\mathscr{E}_R$, and so (26) follows from standard finite element theory.

Let us describe briefly two ideas[2] to improve the error estimates (24)–(26). For that, one has to assume more additional regularity on the right-hand sides.

The first one stems from Nazarov and Plamenevsky [50, Chapter 2]. From their work on the primal fields, one can infer techniques to compute the next principal part(s) of the electric field, i.e. the part which belong(s) to $\mathbf{H}^1(\Omega)$, but not to $\mathbf{H}^2(\Omega)$. This amounts to split further the $\mathbf{H}^1$-regular part of the electric field. In [50, Chapter 2], explicit formulas are built, to derive the coefficients associated to the next principal part(s), for the Laplace operator. In this way, the remaining part of the electric field now belongs to $\mathbf{H}^2(\Omega)$. It can be thus computed with O(h) precision with the continuous, P_1 Lagrange finite elements.

The second idea to improve the convergence rate is to use Dirichlet-to-Neumann techniques in bounded domains, cf. [9,8]. In these papers, one computes the solution with high precision in the neighborhood of the reentrant corners. This technique could be extended easily, so that one also computes the solution – with high accuracy – in a neighborhood of the others corners. Near those corners, the electric field belongs to $\mathbf{H}^1(\Omega)$, but not necessarily to $\mathbf{H}^2(\Omega)$. Then, in the remaining 'exterior' domain (Ω minus those neighborhoods), the solution is computed with a variational formulation, with Dirichlet-to-Neumann operators on the interfaces [9,8].

2.5. The singular complement method in 3D

In general 3D domains, the main difficulty of the *SCM* is to take accurately into account singular subspaces. They originate from geometrical singularities, such as reentrant edges, that can meet at reentrant vertices. In addition to generating infinite dimensional singular subspaces, the challenge is to understand and resolve the links between singular edges and singular vertex functions. Nevertheless, one can proceed with the *SCM* in a number of 3D geometries. We consider successively strong electromagnetic fields around a sharp conical vertex, and then in a prismatic domain, or in a domain, which is invariant by rotation.

2.5.1. Strong fields around a sharp conical vertex

See Fig. 1 for a sketch of a 3D sample domain. It is nonconvex, because of a single, *sharp conical vertex* on its boundary. According to Grisvard [39], the subspace of primal singular fields – with a Dirichlet boundary condition – is of dimension one. Therefore, the dimension of

[2] One could also use mesh refinement techniques. Indeed, on the one hand, the error estimates (24)–(26) are based on regularity results on the regular parts, respectively $\tilde{\mathbf{v}}_S$ and $\tilde{\mathbf{x}}_S$. On the other hand, the error estimate (26) stems from the extra-regularity of $\mathscr{E}_R$. Thus, using suitably graded meshes (see for instance [44]), one could recover an O(h) error estimate. This approach seems worth considering, when one is solving numerically static or stationary problems. However, these techniques are not so practical for the instationary case, since the stability condition would impose much smaller time-steps, because of the grading near reentrant corners.

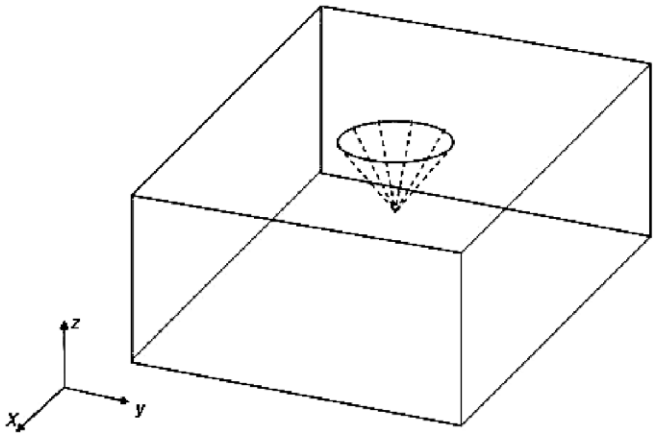

Fig. 1. 3D sample domain with a sharp conical vertex.

the electric singular subspaces $\mathbf{X}_S$, $\mathbf{V}_S$ or $\mathbf{L}_S$ is also one. Compared to a 2D situation, the only novelty is how to compute the singular basis function.

The space of electric fields $\mathbf{X}$ can be split in at least three different direct sums. From a numerical point of view, the choice is made with respect to the ease of implementation. Here, the best choice is

$$\mathbf{X} = \mathbf{X}_R \oplus \mathbf{L}_S.$$

With this choice, the singularities are easily inferred from the primal singular functions (by taking their gradient). Indeed, in 3D, a basis function of $\mathbf{V}_S$ is expressed as the curl of a primal singular *vector* field, i.e. a singular solution of the vector Laplace problem. It is therefore much harder to compute $\mathbf{v}_S$ than $\mathbf{l}_S$.

The singular basis can also be computed by using the *principal part method*. The first step consists of the determination of the principal parts of the dual and primal singular fields. Then, in a second step, one computes basis functions of S_D, Ψ_S and $\mathbf{L}_S$.

The geometrical singularity is *locally* invariant by rotation, see Fig. 1. Let us thus consider the system of spherical coordinates (r, θ, φ), centered at the tip of the cone. Let Γ_{cone} be the part of the boundary which intersects the cone of equation $\theta = w_0/2$, with w_0 the aperture angle of the cone (a priori $\pi < w_0 \leqslant 2\pi$).

As in (6) and (12), let us split s_D – the basis function of S_D – and ψ_S – the basis function of Ψ_S – into the sum of principal and regular parts. It turns out that the principal parts s_D^P and ψ_S^P can be expressed as a sum of separate variable terms. More precisely, they can be written as a sum of spherical harmonic functions, that is terms like

$$r^\mu P_\mu(\cos\theta)\sin(m\varphi) \quad \text{and} \quad r^\lambda P_\lambda(\cos\theta)\sin(n\varphi).$$

Above, $P_\cdot$ is a so-called generalized Legendre function (cf. [1]). Mathematically, it is an eigenfunction of the Laplace–Beltrami operator, related to the eigenvalue

$$-\mu(\mu+1) \text{ or } -\lambda(\lambda+1) \quad \text{with } \mu, \lambda \in \mathbb{R}.$$

The indices m and n depend on the values of μ and λ respectively. Several considerations have to be taken into account to determine the ad hoc values of m, n, μ and λ:

- μ must belong to the interval $]-\frac{3}{2}, -\frac{1}{2}[$, so that s_D^P belongs to $L^2(\Omega)$, but not to $H^1(\Omega)$.
- λ must belong to the interval $]-\frac{1}{2}, \frac{1}{2}[$, so that ψ_S^P belongs to $H^1(\Omega)$, but not to $H^2(\Omega)$.
- Since the boundary Γ_{cone} is locally invariant by rotation, the analyticity in φ of both s_D^P and ψ_S^P requires that the indices m and n be integers.
- To a μ in the admissible interval of μs corresponds only $m = 0$. Similarly, $n = 0$.
- In the system of spherical coordinates, recall that Γ_{cone} is locally defined by $\theta = w_0/2$. Then, λ can be uniquely determined (cf. [13,5]) by solving $P_\lambda(\cos(w_0/2)) = 0$. Using the relation $P_\lambda(\cos\theta) = P_{-\lambda-1}(\cos\theta)$, and in view of the possible intervals for λ and μ, one infers that $\mu = -\lambda - 1$.

Finally, the principal parts read respectively

$$s_D^P = r^\mu P_\mu(\cos\theta) = r^{-\lambda-1} P_\lambda(\cos\theta) \quad \text{and}$$
$$\psi_S^P = r^\lambda P_\lambda(\cos\theta).$$

With the help of the Mathematica software, we computed the behavior of λ, as a function of the angle w_0. For angles lower than a value w_{reg}, λ is greater than 1/2, so that it defines a spherical harmonic function of regularity at least $H^2(\Omega)$. Therefore, only *sharp* conical vertices, i.e. cones for which the aperture is larger than $w_{\text{reg}}/2$, generate a primal singular function. This result is in accordance with the ones obtained in invariant by rotation domains [5,13].

To compute C_ψ, one uses Proposition 2.2, together with (27), to find

$$C_\psi = \frac{\|s_D\|^2}{2\pi(2\lambda+1)\displaystyle\int_0^{w_0/2} P_\lambda(\cos\theta)^2 \sin\theta \, d\theta}.$$

Whereas $\mathbf{l}_S^P$ $(= \nabla\psi_S^P)$'s analytical expression in spherical coordinates is

$$\mathbf{l}_S^P = \lambda r^{\lambda-1} \begin{pmatrix} \dfrac{\cos\varphi}{\sin\theta}\left[P_\lambda(\cos\theta) - \cos\theta P_{\lambda-1}(\cos\theta)\right] \\ \dfrac{\sin\varphi}{\sin\theta}\left[P_\lambda(\cos\theta) - \cos\theta P_{\lambda-1}(\cos\theta)\right] \\ P_{\lambda-1}(\cos\theta) \end{pmatrix}.$$

A numerical implementation is provided in [36].

2.5.2. Strong fields in prismatic, or invariant by rotation, domains

Here, we describe how the *SCM* can be applied in 3D prismatic domains (reentrant edges only), or in 3D, invariant by rotation, domains (*decoupled* reentrant edges and sharp conical vertices). In these cases, one can extend the *SCM* by introducing the *Fourier-singular complement method* (referred to as the *FSCM*).

We focus on the prismatic case: to explain the design of the *FSCM*, let us follow [23] for the variational

formulations, and [27] for the numerical algorithms. In a 3D, invariant by rotation, domain, one can actually proceed by superposing the techniques described before, since one deals here with *decoupled* reentrant edges and sharp conical vertices. One has to replace Refs. [23,27] respectively by [46,28].

We thus solve Maxwell's equations in the domain $\Omega = \Omega_\perp \times]0, L[$, where $\Omega_\perp$ is a 2D polygon. The geometrical singularities are exactly edges parallel to Oz, which correspond to the reentrant corners of $\Omega_\perp$. Since we have to distinguish between functional spaces defined on Ω or on $\Omega_\perp$, we add explicitly the name of the geometrical domain between parentheses.

Let us begin by an important result. On the one hand, according to the splitting *a la Birman and Solomyak* [15,16], there holds $\mathscr{E} = \mathscr{E}_R + \nabla\psi$, with $\mathscr{E}_R \in \mathbf{X}_R(\Omega)$ and $\psi \in \Psi(\Omega)$, the splitting being moreover continuous. On the other hand, it is simple to prove [27, Cor. 3.2] that $\partial_z\psi \in H^1(\Omega)$, for any element of $\Psi(\Omega)$. One concludes that $\mathscr{E}_z$ automatically belongs to $H^1(\Omega)$, so it cannot be *singular*. Thus, one has to concentrate on $\mathscr{E}_\perp = \mathscr{E}_x\vec{e}_x + \mathscr{E}_y\vec{e}_y$.

The second important property, in prismatic domains, is more classical. The Fourier expansion in z can be used to reduce the 3D problem – set in Ω – to a sequence of 2D problems, set in $\Omega_\perp$. Basically, for $u \in L^2(\Omega)$, one writes the usual Fourier expansion

$$u = \sum_{k\geqslant 0} u^k(x,y)\sin\left(\frac{k\pi z}{L}\right) \quad \text{or}$$

$$u = \sum_{k\geqslant 0} u^k(x,y)\cos\left(\frac{k\pi z}{L}\right) \quad \text{with } \|u\|_0^2 = \frac{L}{2}\sum_{k\geqslant 0}\|u^k\|_{0,\Omega_\perp}^2.$$

Thanks to the boundary condition satisfied by $\mathscr{E}$, one chooses

$$\mathscr{E}_x = \sum_{k\geqslant 0}\mathscr{E}_x^k\sin\left(\frac{k\pi z}{L}\right), \quad \mathscr{E}_y = \sum_{k\geqslant 0}\mathscr{E}_y^k\sin\left(\frac{k\pi z}{L}\right),$$

$$\mathscr{E}_z = \sum_{k\geqslant 0}\mathscr{E}_z^k\cos\left(\frac{k\pi z}{L}\right).$$

This allows (cf. [27]) to rewrite the original set of Maxwell's equations as an equivalent sequence (for $k \geqslant 0$) of 2D-MAVFs, acting on

- $\mathscr{E}_\perp^k = \mathscr{E}_x^k\vec{e}_x + \mathscr{E}_y^k\vec{e}_y \in \mathbf{X}(\Omega_\perp)$ and $\mathscr{E}_z^k \in H_0^1(\Omega_\perp)$.
- $p^k \in L^2(\Omega_\perp)$, with $p = \sum_{k\geqslant 0} p^k\sin(k\pi z/L)$ the Lagrange multiplier.

Now, there holds in 2D:

$$\mathbf{X}(\Omega_\perp) = \mathbf{X}_R(\Omega_\perp) \overset{\perp_X}{\oplus} \mathbf{X}_S(\Omega_\perp)$$

with a finite dimensional subspace of singular fields.

In this way, one can use the 2D-*SCM* to compute each Fourier mode $\mathscr{E}_\perp^k$. It is combined to an approximation of the Fourier sequence [44], i.e. by keeping only a finite number of modes, for $0 \leqslant k \leqslant N_F$. This results in the Fourier-singular complement method, where one computes

$$\mathscr{E}^{N_F,h} = \sum_{k=0}^{k=N_F}\left(\mathscr{E}_\perp^{k,h}\sin\left(\frac{k\pi z}{L}\right) + \mathscr{E}_z^{k,h}\cos\left(\frac{k\pi z}{L}\right)\vec{e}_z\right),$$

$$p^{N_F,h} = \sum_{k=0}^{k=N_F} p^{k,h}\sin\left(\frac{k\pi z}{L}\right).$$

Thanks to the finite dimensional character of $\mathbf{X}_S(\Omega_\perp)$, one has to compute a finite number of singular basis functions, once and for all at the initialization stage.

Finally, one may derive error estimates by following the framework developed in [27]. By analogy, provided the data is smooth, using the convergence results of Section 2.4, together with the truncated sequence of Fourier modes, one may reach

$$\|\mathscr{E} - \mathscr{E}^{N_F,h}\|_{\mathbf{X}(\Omega)} \leqslant C\frac{1}{N_F} + C_\varepsilon h^{2\alpha-1-\varepsilon},$$

where C and C_ε are independent of N_F and h, with C_ε like in (26). This estimate could be further improved, following the end of Section 2.4.

3. Numerical experiments

In this section, we present numerical results in order to illustrate the possibilities of the *singular complement method*. In a first part, we compare the three possible splittings of $\mathbf{X}$ (cf. Section 1.2.2), when an electromagnetic wave propagates in a waveguide. In the last part, we propose an example for the coupled Vlasov–Maxwell system of equations.

We do not present any numerical simulation of the singular basis functions. See [8] for the computation of basis functions of $\mathbf{V}_S$ with the help of a substructuring method (and a Dirichlet-to-Neumann boundary operator). See [43] for the computation of basis functions of $\mathbf{V}_S$ using a truncation function. And see [36] for the computation of basis functions of $\mathbf{X}_S$ and $\mathbf{L}_S$. Then, one can find in [6] instances of similar computations in domains, which are invariant by rotation, with the help of the *principal part method*.

As previously mentioned, all computations related to the singular parts – basis functions, matrices, etc. – are carried out at the initialization stage, once and for all, to the exception of the singular coefficients (20). Still, these coefficients require only a constant number of operations to be updated per time-step, as soon as N is fixed. Therefore, the overhead of the *MCS*, in terms of the CPU time or in terms of memory requirements, is very small.

3.1. A comparison of the different splittings

The aim of this subsection is to compare numerically the results obtained with the three splittings of the space of electric fields $\mathbf{X}$, as below

$$\mathbf{X} = \mathbf{X}_R \overset{\perp_X}{\oplus} \mathbf{X}_S, \quad \mathbf{X} = \mathbf{X}_R \oplus \mathbf{V}_S, \quad \mathbf{X} = \mathbf{X}_R \oplus \mathbf{L}_S.$$

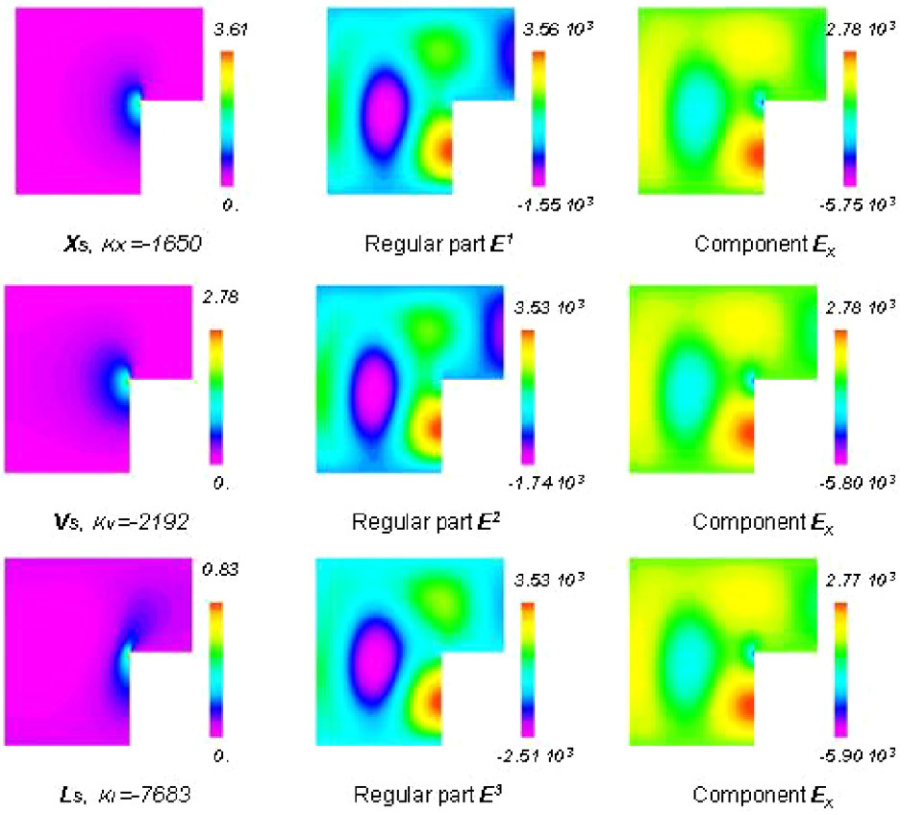

Fig. 2. Singular basis (with their coefficients $\kappa_{\mathbf{x}}$, $\kappa_{\mathbf{v}}$, $\kappa_{\mathbf{l}}$), regular parts and solutions ($\mathscr{E}_x$ component) obtained with the three splittings: $\mathbf{X}_S$ (top), $\mathbf{V}_S$ (medium), $\mathbf{L}_S$ (bottom).

We consider the propagation of a transverse electric wave (or TE mode), in a non-convex geometry.

Let us introduce a step waveguide, and assume that the geometry and data are both independent of the space variable z. The computational domain corresponds to the 2D transverse section, and its geometrical singularities consist of a single reentrant corner, of angle π/α (see Fig. 2). An incoming wave enters the guide through the artificial boundary Γ_A^i, the left-most part of Γ. The waves leaves the guide through the artificial boundary Γ_A^a, the right-most part of Γ. Elsewhere, the boundary is perfectly conducting. As a model, one uses the 2D version of the Silver–Müller absorbing boundary condition (4), that is

$$\mathscr{E}_\perp \cdot \boldsymbol{\tau} + c\mathscr{B}_z = g \quad \text{with } g = C\sin(\omega t) \text{ on } \Gamma_A^i \text{ and } g = 0 \text{ on } \Gamma_A^a.$$

Above, C is a constant, set to $C = 10^4$, and ω is associated to a frequency $\nu = 5\times 10^9$ Hz ($\omega = 2\pi\nu$). At time $t = 0$, there is no electromagnetic field inside the domain. The computation of the electromagnetic field, at times $t > 0$, is achieved through three different expressions of its singular part.

First, by taking the *SCM* with an orthogonal singular part, i.e. with the splitting

$$\mathscr{E}_\perp(t) = \mathscr{E}^1_{\perp R}(t) + \kappa_{\mathbf{x}}(t)\mathbf{x}_S \quad \text{with } \mathbf{x}_S \in \mathbf{X}_S \setminus \{0\}.$$

Second, by taking the *SCM* with a divergence-free singular part, i.e. with the splitting

$$\mathscr{E}_\perp(t) = \mathscr{E}^2_{\perp R}(t) + \kappa_{\mathbf{v}}(t)\mathbf{v}_S \quad \text{with } \mathbf{v}_S \in \mathbf{V}_S \setminus \{0\}.$$

Third, by taking the *SCM* with a curl-free singular part, i.e. with the splitting

$$\mathscr{E}_\perp(t) = \mathscr{E}^3_{\perp R}(t) + \kappa_{\mathbf{l}}(t)\mathbf{l}_S \quad \text{with } \mathbf{l}_S \in \mathbf{L}_S \setminus \{0\}.$$

As we previously mentioned (see Remark 2.4), the regular parts $\mathscr{E}^i_{\perp R}(t)$, $1 \leqslant i \leqslant 3$ are different, even though they all belong to $\mathbf{X}_R$.

The meshsize is such that the 10-point rule is fulfilled, i.e. they are roughly 10 discretization points per wavelength.

We compared the regular and singular parts of the solutions, and the solutions themselves. These tests are conclusive in several ways. We picture (cf. Fig. 2) the isovalues of the regular and singular parts of the component $\mathscr{E}_x$ of the electric field, for the three splittings, after 2.000 time-steps. This corresponds to a real time of $t = 2.0\times 10^{-9}$ s. One can further check that the computed fields are very close from one another, with variations of less than 1.5% in a neighborhood of the reentrant corner. These experiments illustrate the good numerical behavior of the *SCM* in general, and it also shows that the three methods yield very similar results, although they are based on different splittings.

This can be explained by the following argument. In the neighborhood of a reentrant corner, one can provide an expression of each basis function $\mathbf{x}_S, \mathbf{v}_S, \mathbf{l}_S$, in the form of a series. Its first term, *the principal part*, which we denote by **pp**, determines the regularity of the solution. In our case, it belongs to $\mathbf{L}^2(\Omega)$, and not to $\mathbf{H}^1(\Omega)$. In [36], it has been proven that the principal part is the same for all basis functions, up to a multiplicative constant. In our example, it reads

$$\mathbf{pp} = r^{\alpha-1}(\sin(\alpha\theta)\vec{e}_r + \cos(\alpha\theta)\vec{e}_\theta)$$

with $(\vec{e}_r, \vec{e}_\theta)$ the canonical basis associated to the polar coordinates, centered at the reentrant corner. The principal part is divergence- and curl-free. But it does not satisfies the homogeneous tangential trace boundary condition, otherwise it would be zero. One can then split each basis function like

1. $\mathbf{x}_S = c_\mathbf{x}\mathbf{pp} + \mathbf{F}_\mathbf{x}$, with $\mathbf{F}_\mathbf{x} \in \mathbf{H}^1(\Omega)$. This field verifies $\mathbf{F}_\mathbf{x} \cdot \boldsymbol{\tau}_{|\Gamma} = -\mathbf{pp} \cdot \boldsymbol{\tau}_{|\Gamma}$, and also enforces the orthogonality condition $(\mathbf{F}_\mathbf{x}, \mathbf{x}_R)_\mathbf{X} = 0$, $\forall \mathbf{x}_R \in \mathbf{X}_R$.
2. $\mathbf{v}_S = c_\mathbf{v}\mathbf{pp} + \mathbf{F}_\mathbf{v}$, with $\mathbf{F}_\mathbf{v} \in \mathbf{H}^1(\Omega)$. This field verifies $\mathbf{F}_\mathbf{v} \cdot \boldsymbol{\tau}_{|\Gamma} = -\mathbf{pp} \cdot \boldsymbol{\tau}_{|\Gamma}$, and also enforces the orthogonality condition $(\mathbf{F}_\mathbf{v}, \mathbf{v}_R)_\mathbf{X} = 0$, $\forall \mathbf{v}_R \in \mathbf{V}_R$.
3. $\mathbf{l}_S = c_\mathbf{l}\mathbf{pp} + \mathbf{F}_\mathbf{l}$, with $\mathbf{F}_\mathbf{l} \in \mathbf{H}^1(\Omega)$. This field verifies $\mathbf{F}_\mathbf{l} \cdot \boldsymbol{\tau}_{|\Gamma} = -\mathbf{pp} \cdot \boldsymbol{\tau}_{|\Gamma}$, and also enforces the orthogonality condition $(\mathbf{F}_\mathbf{l}, \mathbf{l}_R)_\mathbf{X} = 0$, $\forall \mathbf{l}_R \in \mathbf{L}_R$.

In a neighborhood of the reentrant corner, the precision of the numerical method depends essentially on the quality of the approximation of the principal part. But according to the error estimates on the constants, in Section 2.4, it is very good in all cases. This explains why the basis functions are accurately computed, at least in terms of their principal part. What our experiments show *in addition*, is that this initial precision is maintained over a large number of time-steps, when the coefficients $\kappa_\mathbf{x}(t)$, $\kappa_\mathbf{v}(t)$ and $\kappa_\mathbf{l}(t)$ are computed.

Remark 3.1

- For simplicity reasons, the electric field in the above example is divergence-free. Nonetheless, one would reach similar conclusions for an L^2 divergence field. We refer the reader to [36, Chapter 9].
- One might think that the splitting within the divergence-free subspace $\mathbf{V}$ is better suited. The example shows that it is not the case. As it happens, it is equivalent to enforce $\mathrm{div}\mathscr{E}^2_{\perp_R}(t) = 0$, $\mathrm{div}\mathscr{E}^1_{\perp_R}(t) = -\kappa_1(t)\mathrm{div}\,\mathbf{x}_S$ or $\mathrm{div}\mathscr{E}^3_{\perp_R}(t) = -\kappa_3(t)\mathrm{div}\,\mathbf{l}_S$.

In conclusion, it appears that the three splittings provide very similar numerical results. Therefore, the choice between the three splittings ought to be made with respect to the simpler variational formulation, and/or to the ease of implementation.

3.2. A Vlasov–Maxwell implementation

We focus now on the numerical solution of the coupled Vlasov–Maxwell system of equations. Recall that Vlasov equation models the transport of charged particles, under the influence of an electromagnetic field. The Vlasov equation reads

$$\frac{\partial f}{\partial t} + \mathbf{v} \cdot \nabla_\mathbf{x} f + \frac{\mathbf{F}}{m} \cdot \nabla_\mathbf{v} f = 0.$$

Above, the unknown f is the distribution function of the particles, $f(\mathbf{x}, \mathbf{v}, t)$, $\mathbf{v}$ stands for the velocities of the particles, m is the mass of a particle, and $\mathbf{F}$ is the applied force. The coupling occurs

- on the one hand, by the right-hand sides of Maxwell equations, ρ and $\mathscr{J}$, which are computed from the solution to the Vlasov equation $f(\mathbf{x}, \mathbf{v}, t)$, thanks to the relations
$$\rho = \int_\mathbf{v} f \,\mathrm{d}\mathbf{v}, \quad \mathscr{J} = \int_\mathbf{v} f\mathbf{v}\,\mathrm{d}\mathbf{v},$$
- on the other hand, the electromagnetic field $(\mathscr{E}, \mathscr{B})$ determines the forces that act on the particles in the Vlasov model, via the well-known Lorentz force $\mathbf{F}$
$$\mathbf{F} = e(\mathscr{E} + \mathbf{v} \times \mathscr{B}).$$
Geometrical singularities have no effect per se on the regularity of the solution to the Vlasov equation (cf. [51]). Therefore, the numerical methods, which are classically used, require marginal modifications. In our case, we resort to a particle method [11], which consists in approximating the distribution function $f(\mathbf{x}, \mathbf{v}, t)$ by a linear combination of Dirac masses.

However, these geometrical singularities have an influence over f, through the *coupling*. In other words, the Lorentz force $\mathbf{F}$ must be computed accurately. Otherwise, the trajectories of the charged particles are incorrect, as so are their positions and velocities. Then, ρ and $\mathscr{J}$ are incorrect, and so there's no chance to capture the true solution. This is the reason why we compare once more the two numerical implementations, with and without *SCM*.

We consider an L-shaped domain Ω, and assume its boundary is entirely perfectly conducting. Initial conditions are uniformly set to zero. At this time, a bunch of particles – electrons – is emitted from the top-most part of the boundary, with an initial velocity equal to $\mathbf{v} = v_y\vec{e}_y$, with $v_y = -2 \times 10^8\ \mathrm{m\ s^{-1}}$. The electromagnetic field is therefore a *self-consistent* field. Particles are absorbed at the down-most part of the boundary.

The *SCM* is implemented with the splitting $\mathbf{X} = \mathbf{X}_R \overset{\perp_\mathbf{X}}{\oplus} \mathbf{X}_S$.

As shown in Fig. 3a, the electric field – $\mathscr{E}_x$ component – obtained after 500 time-steps is very different, when it is computed with and without the *SCM*. Recall that the electromagnetic field is the result of the motion of the charged

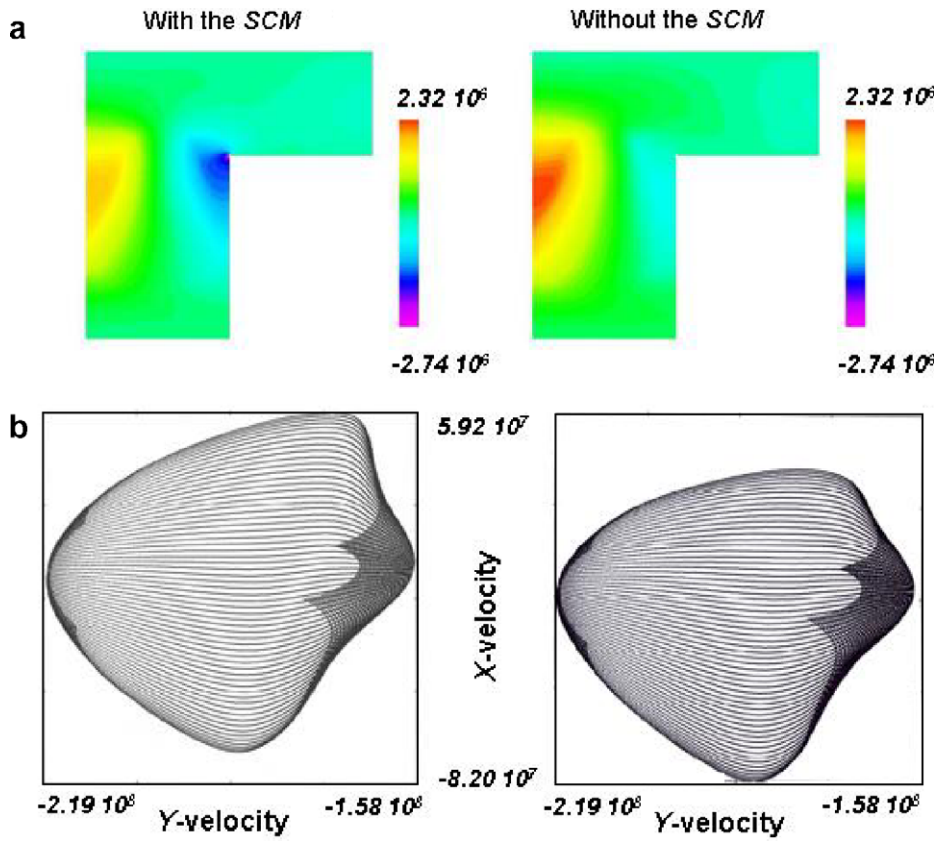

Fig. 3. (a)Vlasov–Maxwell simulation. Computed solutions ($\mathscr{E}_x$ component) obtained with (left) and without (right) the *SCM*. (b) Vlasov–Maxwell simulation. Distributions between v_y and v_x components of the particle velocities.

particles only. Therefore, differences are entirely due to the coupling between the Vlasov and Maxwell equations.

In parallel to these differences between the two computed electromagnetic fields, one also observes an error, in terms of the general trends of the motions of the particles. Without the *SCM*, the bunch is 'flattened' (wrt the *SCM* implementation). See Fig. 3b, where the distributions between v_y and v_x components of the velocities are represented, at the same time-step. Via the coupling, these discrepancies have an impact on the trajectories of the particles. The bunch is 'widening' too much over the time iterations, and some particles are absorbed by the left and right parts of the boundary. With the *SCM*, this phenomenon does not occur.

4. Conclusion

In this paper, we considered the solution of the instationary Maxwell equations with charges, in domains with singular geometries. This model actually stems from the solution to the coupled Vlasov–Maxwell system of equations, for which, in essence, the electric field is not divergence-free [10].

To that aim, we studied direct, and possibly orthogonal, splittings of the space of electromagnetic fields, thus defining extensions of the *singular complement method*. In particular, we focused on singular electromagnetic fields with a $L^2(\Omega)$ non-vanishing divergence. The mappings, which relate those singular fields to the primal and dual singularities of the (vector) Laplace operator, have been very helpful for carrying out our analysis.

This paper is a generalization of previous works, aimed at solving the divergence-free electromagnetic problems. One of the foremost result is that all the splittings provide the same principal part, which allows to choose between them, from an implementation point of view.

As far as numerical experiments are concerned, we point to the implementation of our original model, i.e. the Vlasov–Maxwell system of equations.

As we emphasized, the theory can be further applied to the case of infinite dimensional singular subspaces, provided they originate from reentrant edges only [23], or from decoupled reentrant edges and reentrant vertices [46]. However, one has still to propose a satisfactory extension of the *singular complement method* to handle the most general 3D case, that is when reentrant edges meet at a reentrant vertex. In this respect, the functional frameworks developed in [33,22,26] are promising, in the sense that they allow for a *continuous* approximation of the total electric field.

References

[1] M. Abramowitz, I.A. Stegun, Handbook of Mathematical Functions, Dover Publications, Inc., New York, 1970.

[2] F. Assous, P. Ciarlet Jr., A characterization of the orthogonal of $\Delta(H^2(\Omega) \cap H_0^1(\Omega))$ in $L^2(\Omega)$, C.R. Acad. Sci. Paris, Ser. I 325 (1997) 605–610.

[3] F. Assous, P. Ciarlet Jr., Modèles et méthodes pour les équations de Maxwell, Technical Report ENSTA 349, ENSTA, Paris, France, 2002 (in French).

[4] F. Assous, P. Ciarlet Jr., E. Garcia, Singular electromagnetic fields: inductive approach, C.R. Acad. Sci. Paris, Ser. I 341 (2005) 605–610.

[5] F. Assous, P. Ciarlet Jr., S. Labrunie, Solution of axisymmetric Maxwell equations, Math. Methods Appl. Sci. 26 (2003) 861–896.

[6] F. Assous, P. Ciarlet Jr., S. Labrunie, J. Segré, Numerical solution to the time-dependent Maxwell equations in axisymmetric singular domain: the singular complement method, J. Comput. Phys. 191 (2003) 147–176.

[7] F. Assous, P. Ciarlet Jr., P.A. Raviart, E. Sonnendrücker, A characterization of the singular part of the solution to Maxwell's equations in a polyhedral domain, Math. Methods Appl. Sci. 22 (1999) 485–499.

[8] F. Assous, P. Ciarlet Jr., J. Segré, Numerical solution to the time-dependent Maxwell equations in two-dimensional singular domain: the singular complement method, J. Comput. Phys. 161 (2000) 218–249.

[9] F. Assous, P. Ciarlet Jr., E. Sonnendrücker, Resolution of the Maxwell equations in a domain with reentrant corners, Math. Mod. Numer. Anal. 32 (1998) 359–389.

[10] F. Assous, P. Degond, E. Heintzé, P.A. Raviart, J. Segré, On a finite element method for solving the three-dimensional Maxwell equations, J. Comput. Phys. 109 (1993) 222–237.

[11] F. Assous, P. Degond, J. Segré, A particle-tracking method for 3D electromagnetic PIC codes on unstructured meshes, Comput. Phys. Com. 72 (1992) 105–114.

[12] I. Babuska, The finite element method with Lagrange multipliers, Numer. Math. 20 (1973) 179–192.

[13] C. Bernardi, M. Dauge, Y. Maday, Spectral Methods for Axisymmetric Domains, Series in Applied Mathematics, Gauthiers-Villlars, Paris and North Holland, Amsterdam, 1999.

[14] C.K. Birdsall, A.B. Langdon, Plasmas Physics via Computer Simulation, MacGraw-Hill, New-York, 1985.

[15] M.Sh. Birman, M.Z. Solomyak, L^2-theory of the Maxwell operator in arbitrary domains, Russ. Math. Surveys 42 (1987) 75–96.

[16] M.Sh. Birman, M.Z. Solomyak, The Weyl asymptotic decomposition of the spectrum of the Maxwell operator for domain with lipschitzian boundary, Vestnik. Leningr. Univ. Math. 20 (1987) 15–21.

[17] M.Sh. Birman, M.Z. Solomyak, On the main singularities of the electric component of the electro-magnetic field in region with screens, St. Petersburg Math. J. 5 (1994) 125–139.

[18] A.-S. Bonnet-Ben Dhia, C. Hazard, S. Lohrengel, A singular field method for the solution of Maxwell's equations in polyhedral domains, SIAM J. Appl. Math. 59 (1999) 2028–2044.

[19] F. Brezzi, On the existence, uniqueness and approximation of saddle point problems arising from Lagrange multipliers, RAIRO Anal. Numér. (1974) 129–151.

[20] A. Buffa, P. Ciarlet Jr., On traces for functional spaces related to Maxwell's equations. Part I: An integration by parts formula in Lipschitz polyhedra, Math. Methods Appl. Sci. 24 (2001) 9–30.

[21] P. Ciarlet, Basic error estimates for elliptic problems, in: P. Ciarlet, J.-L. Lions (Eds.), Handbook of Numerical Analysis, vol. II, North Holland, 1991, pp. 17–352.

[22] P. Ciarlet Jr., Augmented formulations for solving Maxwell equations, Comput. Methods Appl. Mech. Engrg. 194 (2005) 559–586.

[23] P. Ciarlet Jr., E. Garcia, J. Zou, Solving Maxwell equations in 3D prismatic domains, C.R. Acad. Sci. Paris, Ser. I 339 (2004) 721–726.

[24] P. Ciarlet Jr., V. Girault, *Inf–sup* condition for the 3D, P_2-iso-P_1, Taylor–Hood finite element; application to Maxwell equations, C.R. Acad. Sci. Paris, Ser. I 335 (2002) 827–832.

[25] P. Ciarlet Jr., J. He, The singular complement method for 2D scalar problems, C.R. Acad. Sci. Paris, Ser. I 336 (2003) 353–358.

[26] P. Ciarlet Jr., E. Jamelot, Continuous Galerkin methods for solving Maxwell equations in 3D geometries, submitted to the Proceedings of ENUMATH'05.

[27] P. Ciarlet Jr., B. Jung, S. Kaddouri, S. Labrunie, J. Zou, The Fourier singular complement method for the Poisson problem. Part I: prismatic domains, Numer. Math. 101 (2005) 423–450.

[28] P. Ciarlet Jr., B. Jung, S. Kaddouri, S. Labrunie, J. Zou, The Fourier Singular Complement Method for the Poisson problem. Part II: axisymmetric domains, Numer. Math. 102 (2005) 588–610.

[29] M. Costabel, A remark on the regularity of solutions of Maxwell's equations on Lipschitz domains, Math. Methods Appl. Sci. 12 (1990) 365–368.

[30] M. Costabel, A coercive bilinear form for Maxwell's equations, J. Math. Anal. Appl. 157 (1991) 527–541.

[31] M. Costabel, M. Dauge, Maxwell and Lamé eigenvalues on polyhedral domains, Math. Methods Appl. Sci. 22 (1999) 243–258.

[32] M. Costabel, M. Dauge, Singularities of electromagnetic fields in polyhedral domains, Arch. Rational Mech. Anal. 151 (2000) 221–276.

[33] M. Costabel, M. Dauge, Weighted regularization of Maxwell equations in polyhedral domains, Numer. Math. 93 (2002) 239–277.

[34] M. Dauge, Elliptic Boundary Value Problems on Corner Domains, Lecture Notes in Mathematics, vol. 1341, Springer-Verlag, Berlin, 1988.

[35] M. Fortin, R. Glowinski, Augmented Lagrangian Methods, Springer Series in Computational Mathematics, vol. 5, 1986.

[36] E. Garcia, Résolution des équations de Maxwell avec charges dans des domaines non convexes, PhD Thesis, University Paris 6, France, 2002 (in French).

[37] E. Garcia, S. Labrunie, Régularité spatio-temporelle de la solution des équations de Maxwell dans des domaines non convexes, C.R. Acad. Sci. Paris, Ser. I 334 (2002) 293–298.

[38] V. Girault, P.A. Raviart, Finite Element Methods for Navier–Stokes Equations, Series in Computational Mathematics, vol. 5, Springer-Verlag, Berlin, 1986.

[39] P. Grisvard, Elliptic Problems in Nonsmooth Domains, Monographs and Studies in Mathematics, vol. 24, Pitman, London, 1985.

[40] P. Grisvard, Singularities in Boundary Value Problems, vol. 22, RMA Masson, Paris, 1992.

[41] W.W. Hager, Updating the inverse of a matrix, SIAM Rev. 31 (1989) 221–239.

[42] C. Hazard, Numerical simulation of corner singularities: a paradox in Maxwell-like problems, C.R. Acad. Sci. Paris, Ser. IIb 330 (2002) 57–68.

[43] C. Hazard, S. Lohrengel, A singular field method for Maxwell's equations: numerical aspects for 2D magnetostatics, SIAM J. Appl. Math. 40 (2002) 1021–1040.

[44] B. Heinrich, The Fourier-finite element method for Poisson's equation in axisymmetric domains with edges, SIAM J. Numer. Anal. 33 (1996) 1885–1911.

[45] E. Jamelot, A nodal finite element method for Maxwell's equations, C.R. Acad. Sci. Paris, Ser. I 339 (2004) 809–814.

[46] S. Labrunie, La méthode du complément singulier avec Fourier pour les équations de Maxwell en domaine axisymétrique, Technical Report Institut Elie Cartan 2004-42, Nancy, Paris, France, 2004 (in French).

[47] S. Lohrengel, Etude mathématique et résolution numérique des équations de Maxwell dans un domaine non régulier, PhD Thesis, University Paris 6, France, 1998 (in French).

[48] M. Moussaoui, Sur l'approximation des solutions du problème de Dirichlet dans un ouvert avec coins, in: P. Grisvard et al. (Eds.), Singularities and Constructive Methods for Their Treatment, vol. 1121, Springer-Verlag, 1984, pp. 199–206 (in French).

[49] K. Müller, Foundations of the Mathematical Theory of Electromagnetic Waves, Springer-Verlag, Berlin, 1969.
[50] S.A. Nazarov, B.A. Plamenevsky, Elliptic problems in domains with piecewise smooth boundaries, De Gruyter Expositions Math. 13 (1994).
[51] P.A. Raviart, An Analysis of Particle Methods, Springer-Verlag, Berlin, 1985.
[52] C. Weber, A local compactness theorem for Maxwell's equations, Math. Methods Appl. Sci. 2 (1980) 12–25.